Figure 1: A rotated figure

Model 0.1: Test

$$
\begin{aligned}
T_{cc,out},\, C_e,\, C_w,\, T_{c,out} = \text{combined cooler model}(q_c, R_p, R_s, \omega_{dc}, \omega_{wct}, T_{amb}, HR_i, T_v, \dot{m}_v)\\
T_{cc,in} &= T_{c,out}\\
T_{dc,in} &= T_{cc,in}\\
q_{dc} &= q_c \cdot (1 - R_p)\\
q_{wct,p} &= q_c \cdot R_p\\
q_{wct,s} &= q_{dc} \cdot R_s\\
T_{dc,out},\, C_{e,dc} &= \text{dc model}(q_{dc},\, \omega_{\mathrm{dc}},\, T_{\mathrm{amb}},\, T_{dc,in})\\
q_{wct},\, T_{wct,in} &= \text{mixer model}(q_{wct,p},\, T_{Tcc,in},\, q_{wct,s},\, T_{dc,out})\\
T_{wct,out},\, C_{e,wct},\, C_{w,wct} &= \text{wct model}(q_{wct},\, \omega_{wct},\, T_{amb},\, HR,\, T_{wct,in})\\
T_{c,in},\, T_{c,out} &= \text{condenser model}(q_c,\, \dot{m}_v,\, T_v)\\
q_{cc},\, T_{cc,out} &= \text{mixer model}(q_{wct},\, T_{wct,out},\, q_{dc},\, T_{dc,out})\\
C_e &= C_{e,dc} + C_{e,wct} + C_{e,c}\\
C_w &= C_{w,wct}
\end{aligned}
$$

As can be seen in Model 0.1, the counter is working.

Problem .1: Test

Hello, here is some text without a meaning. This text should show what a printed text will look like at this place. If you read this text, you will get no information. Really? Is there no information? Is there a difference between this text and some nonsense like “Huardest gefburn”? Kjift – not at all! A blind text like this gives you information about the selected font, how the letters are written and an impression of the look. This text should contain all letters of the alphabet and it should be written in of the original language. There is no need for special content, but the length of words should match the language.

$$\min_{\mathbf{x},\,\mathbf{e};\,\theta} \quad J = f(\mathbf{x}, \mathbf{e}; \theta) = f(x)$$

with:

- Model name model

$$out_1,\, out_2 = f(in_1,\, in_2,\, \dots,\, in_N)$$

- Decision variables

$$\mathbf{x} = [x_1,\, x_2]$$

- Environment variables

$$\mathbf{e} = [e_1,\, e_2,\, \dots,\, e_3]$$

- Fixed parameters

$$\theta = [\theta_1 = X,\, \theta_2 = Y]$$

subject to:

- Box-bounds
  - $x_1 \in [\underline{x}_1, \overline{x}_1]$

- $x_2 \in [\underline{x}_2, \overline{x}_2]$

▸ Constraints

- $|out_X - out_Y| \leq \epsilon_1$
- $out_X \leq out_Z - \Delta Z$

As can be seen in Problem .1, the counter is working.

TL;DR

test test

Problem: Test

$$\min_{\mathbf{x}, \mathbf{e}; \theta} \quad J = f(\mathbf{x}, \mathbf{e}; \theta) = f(x)$$

with:

- Model name model
$$out_1,\ out_2 = f(in_1,\ in_2,\ \dots,\ in_N)$$
- Decision variables
$$\mathbf{x} = [x_1,\ x_2]$$
- Environment variables
$$\mathbf{e} = [e_1,\ e_2,\ \dots,\ e_3]$$
- Fixed parameters
$$\theta = [\theta_1 = X,\ \theta_2 = Y]$$

subject to:

- Box-bounds
  - $x_1 \in [\underline{x}_1, \overline{x}_1]$
  - $x_2 \in [\underline{x}_2, \overline{x}_2]$
- Constraints
  - $|out_X - out_Y| \leq \epsilon_1$
  - $out_X \leq out_Z - \Delta Z$

The kaobook class

PhD Thesis

Towards optimal resource management in solar thermal applications: desalination and CSP

Juan Miguel Serrano Rodríguez

June 16, 2025

University of Almería

The kaobook class

Disclaimer
You can edit this page to suit your needs. For instance, here we have a no copyright statement, a colophon and some other information. This page is based on the corresponding page of Ken Arroyo Ohori's thesis, with minimal changes.

Colophon
This document was typeset with the help of KOMA-Script and LaTeX using the kaobook class.
The source code of this book is available at:
https://github.com/fmarotta/kaobook
(You are welcome to contribute!)

Publisher
First printed in May 2019 by University of Almería

The harmony of the world is made manifest in Form and Number, and the heart and soul and all the poetry of Natural Philosophy are embodied in the concept of mathematical beauty.

– D’Arcy Wentworth Thompson

Acknowledgements

Test test test

Federico Marotta

Summary

I am of the opinion that every LaTeX geek, at least once during his life, feels the need to create his or her own class: this is what happened to me and here is the result, which, however, should be seen as a work still in progress. Actually, this class is not completely original, but it is a blend of all the best ideas that I have found in a number of guides, tutorials, blogs and tex.stackexchange.com posts. In particular, the main ideas come from two sources:

- Ken Arroyo Ohori's Doctoral Thesis, which served, with the author's permission, as a backbone for the implementation of this class;
- The Tufte-Latex Class, which was a model for the style.

The first chapter of this book is introductory and covers the most essential features of the class. Next, there is a bunch of chapters devoted to all the commands and environments that you may use in writing a book; in particular, it will be explained how to add notes, figures and tables, and references. The second part deals with the page layout and design, as well as additional features like coloured boxes and theorem environments.

I started writing this class as an experiment, and as such it should be regarded. Since it has always been intended for my personal use, it may not be perfect but I find it quite satisfactory for the use I want to make of it. I share this work in the hope that someone might find here the inspiration for writing his or her own class.

Resumen

Contents

List of Figures

List of Tables

List of Listings

How to read this thesis

TL;DR

This preliminary chapter explains how to read this thesis, mainly the different environment boxes used throughout the manuscript, why the large margins, what is placed in them, and how to use the interactive features of the manuscript. This is an example of a Too Long; Didn't Read (TL;DR) box. It contains an Abstract/Summary of the main point of the chapter and are placed at the beginning of every chapter.

This LaTeX template is designed with large margins, on the one hand this allows to have shorter lines, which makes for an easier reading experience but most interestingly, it also allows to place additional information in the margins, such as side notes, side citations, figures, tables... your imagination is the limit! Or rather LaTeX compilation errors and your patience are. Throughout this manuscript I will add side notes[1] to provide additional information and comments that would otherwise be too distracting and verbose to include in the main text, constantly interrupting the flow of the reading. The side notes are not essential to understand the content of the document, but mostly complementary.

1: Like this one! They are like footnotes, but placed in the margin of the page

Boxed environments

Both problem definition boxes (*e.g.* ref) and model definition boxes (*e.g.* Model 0.2) are countered environments and can (and will) be referenced in the text.

Figure 2: Example figure. Try clicking or scanning the QR code to access the interactive version.

Problem: Problem definition box example

This is an example of a problem definition box. It is used to formally and concisely define an optimization problem.

$$\min_{\mathbf{x},\mathbf{e};\theta} \quad J = f(\mathbf{x}, \mathbf{e}; \theta) = XXXX$$

with:

$$out_1, out_2 = f(in_1, in_2, \dots, in_N)$$
$$out_1, out_2 = f(in_1, in_2, \dots, in_N)$$

- Decision variables
$$\mathbf{x} = [x_1, x_2]$$
- Environment variables
$$\mathbf{e} = [e_1, e_2, \dots, e_3]$$
- Fixed parameters
$$\theta = [\theta_1 = X, \theta_2 = Y]$$

subject to:

- Box-bounds
  - $x_1 \in [\underline{x}_1, \overline{x}_1]$
  - $x_2 \in [\underline{x}_2, \overline{x}_2]$
- Constraints

- $|out_X - out_Y| \leq \epsilon_1$
- $out_X \leq out_Z - \Delta Z$

Model 0.2: Model definition box example

$$out_1, out_2 = \text{some cool model}(in_1, in_2, in_3)$$

Other boxes

Other boxes are used to highlight important points, or to provide additional information that is not essential to the main text.

In order to make the book more interactive and link-friendly, I have enabled hyperlinks in the PDF. This means that you can click on the references, citations, and links to external resources, and they will take you to the corresponding location. This is standard latex, however to maintain a consistent experience in the physical version, QR codes are inserted in the margin next to the links. The reader is invited to scan them with a QR code reader to access the corresponding online resource[2]. Some figures also include QR codes that link to an interactive (HTML) version of the figure, see Figure 2 as an example.

The additional material as well as the source code of this document are hosted in a Zenodo repository[3]. Alternatively, a mirror repository is also available at:

https://github.com/juan11iguel/my-thesis

It seems unlikely that both Zenodo and GitHub will go down at a time where this document is still relevant, and if they do, I think there will be more important things to worry about than losing access to the interactive content of this thesis.

2: I believe that this is a good way to make the document more accessible and to encourage readers to explore the content in more depth. However, the interactive features are **optional** and not necessary to understand the content of the document.

3:

: Like hoarding toilet paper

About the author

Un payaso

– Lidia Roca, probablemente

I am currently completing my PhD thesis, with the defense planned for October. My research interests lie primarily in automatic control, optimization, and robotics, especially as applied to solar thermal processes.

I think I am mostly a creative person, but in order to implement those ideas, throughout my work, I've gained experience with a variety of tools and technologies, including Linux, Python, Docker, LaTeX, and the Robot Operating System (ROS). I'm particularly passionate about open science and open source software, and I strive to contribute to communities that value transparency and collaboration.

For my bachelor's thesis, I created a mobile robotics lab in the University of Almería by deploying the Duckietown project. This gave me the opportunity to interact and work with ROS, and since the whole project was deployed using Docker, to learn about containerization technologies. For my master's thesis, work was also software-related, but this time it was about the implementation of a SCADA-like system using Python. During my PhD, I have had four years to really delve into these technologies, so today they are an integral part of my workflow and I am confident to say they've helped me become effective at implementing those (sometimes too) many ideas.

Lidia esto solo lo he copiado por tener algo, ya lo mejoraré

Introduction

1 Context and motivation

asdad

2 Thermal desalination overview

Desalination is increasingly recognized as a key strategy to address global freshwater scarcity, driven by the combined pressures of climate change and population growth. Regions already facing drought and water stress, such as parts of Spain, are expected to see growing dependence on desalinated water to meet rising demand. While desalination technologies—particularly membrane-based systems like Reverse Osmosis (RO)—have seen rapid expansion, the energy intensity of the process remains a major challenge. To mitigate this, efforts have focused on improving energy efficiency and integrating renewable energy sources such as solar or geothermal heat. In particular, thermal desalination technologies like Multi-Effect Distillation (MED) are gaining renewed interest due to their compatibility with low-exergy heat sources (*e. g.* waste heat) and the ability to treat high-salinity brines. These thermal processes also align better with circular economy approaches, allowing the concentration of brine and the recovery of valuable minerals such as lithium or magnesium, an emerging field known as brine mining.

CSP overview | 3

In the pursuit of eliminating reliance on fossil fuels sources for energy generation and replacing them by renewable sources, Concentrated Solar Power (CSP) has proven to be a reliable contributor. In particular, in providing much needed energy storage, dispatchability and ensuring grid stability.

CSP plants use mirrors to concentrate the sun's energy to finally drive a turbine that generates electricity. This technology currently represents a minor part of renewable energy generation in Europe. Only approximately 5 GW are installed globally (of which 2.3 GW in Europe are concentrated in Spain). However, the potential for growth is significant given the capability of CSP to provide renewable electricity when needed thanks to in-built energy storage continuing the production even in the absence of sunlight, unlike other renewable technologies that are dependent on the availability of the energy source. Of increasing importance is also their potential application in improving the manageability of the grid, replacing fossil fuel alternatives. Their dispatchability enables plants to respond to peaks in demand, and provide ancillary services to the grid. According to the International Energy Agency forecasts, CSP has a huge potential in the long term, ranging from the 986 TWh by 2030 up to 4186 TWh by 2050 [1], which means that CSP will account for 11% of the electricity generated worldwide and for 4% in the case of Europe.

[1]: IEA (2014), *Energy Technology Perspectives*

3.1 Water use

The cooling of the power block in this technology plays a crucial role in its feasibility. The cheapest and most efficiency cooling technology is evaporative cooling, and that is why most plants, specially in Spain where built using this alternative (XX % [2]), however, the high-radiation areas in which they are located are usually regions with rapidly-degrading water availability due to climate change, so water has become a scarce resource. Nowadays most likely those plants would have been built with dry cooling technologies, significantly increasing the cost (up to 8% during periods of high ambient temperatures when energy demand and prices peak [**<empty citation>**]).

[2]: Thonig et al. (2023), *CSP.Guru 2023-07-01*

<empty citation>

4 Cooling overview

CSP plants are, in general, located in arid areas, where sun irradiance is high but water is scarce. The efficiency of these plants is highly dependent on the temperature at which the steam is condensed. To date, the conventional systems used to remove excess heat from CSP plants are either wet (water-cooled) or dry (air-cooled). The lowest attainable condensing temperature is achieved in wet cooling systems that depend on the wet-bulb temperature, allowing CSP plants to achieve higher efficiencies. However, this efficiency increase is at the expense of a high cost: excessive water use. Dry cooling systems eliminate the water use but they lead to lower plant efficiencies when the ambient air temperature is high. Those hot periods are often the periods of peak system demand and higher electricity sale price. The combination of the advantages of each of them into an innovative cooling system is thus of great interest. There are different types of innovative cooling systems: those that integrate the dry and wet cooling systems into the same cooling device, which are called hybrid cooling systems [3–5] and those that combine separate dry and wet cooling systems, which are called combined cooling systems. In the case of hybrid cooling systems, the dry section are composed of compact heat exchangers included in a wet cooling tower [3]. This kind of cooling systems can be considered as an efficient cooling solution for CSP plants [6] due to the energy conservation and water and greenhouse gas emissions savings. In the case of combined cooling systems, different configurations can be found. The most commonly proposed in the literature is the one that considers an Air-Cooled Condenser (ACC) in parallel with a WCT, as can be seen in [7, 8]. In this kind of configuration, the exhaust steam from the turbine is condensed either through the ACC or through a Surface Condenser (SC) coupled with the WCT. Another configuration, recently proposed in [9] is a wet cooling tower and a DC (type Air-Cooled Heat Exchanger (ACHE)) sharing a surface condenser. In this case, the exhaust steam from the turbine is condensed through the surface condenser and the heated cooling water is cooled either through the WCT or through the dry cooler. This kind of combined cooling systems are proposed as the most suitable option for a flexible operation as a function of the ambient conditions, since they allow to select the best operation strategies to achieve an optimum water and electricity consumption compromise [10]. In addition, if the optimization is combined with energy demand forecasting as described in [11], the expected results can be even better.

[3]: Rezaei et al. (2010), "Reducing Water Consumption of an Industrial Plant Cooling Unit Using Hybrid Cooling Tower"

[4]: Asvapoositkul et al. (2014), "Comparative Evaluation of Hybrid (Dry/Wet) Cooling Tower Performance"

[5]: Hu et al. (2018), "Thermodynamic Characteristics of Thermal Power Plant with Hybrid (Dry/Wet) Cooling System"

[6]: El Marazgioui et al. (2022), "Impact of Cooling Tower Technology on Performance and Cost-Effectiveness of CSP Plants"

[7]: Barigozzi et al. (2011), "Wet and Dry Cooling Systems Optimization Applied to a Modern Waste-to-Energy Cogeneration Heat and Power Plant"

[8]: Barigozzi et al. (2014), "Performance Prediction and Optimization of a Waste-to-Energy Cogeneration Plant with Combined Wet and Dry Cooling System"

[9]: Palenzuela et al. (2022), "Experimental Assessment of a Pilot Scale Hybrid Cooling System for Water Consumption Reduction in CSP Plants"

[10]: Asfand et al. (2020), "Thermodynamic Performance and Water Consumption of Hybrid Cooling System Configurations for Concentrated Solar Power Plants"

[11]: Wazirali et al. (2023), "State-of-the-Art Review on Energy and Load Forecasting in Microgrids Using Artificial Neural Networks, Machine Learning, and Deep Learning Techniques"

5 Modelling overview

5.1 Performance metrics

To evaluate the quality of the models fit to the experimental data, four performance metrics were evaluated: coefficient of determination (R^2), RMSE, Mean Absolute Error (MAE) and Mean Absolute Percentage Error (MAPE). These metrics are described below.

Coefficient of determination. R^2 measures the proportion of the variance in the predicted variable that can be attributed to the independent variable(s), in this case the considered system inputs. Values close to one indicate a better prediction accuracy. It is calculated as follows:

$$R^2 = 1 - \frac{\sum_{i=1}^{n}(y_i - \hat{y}_i)^2}{\sum_{i=1}^{n}(y_i - \bar{y})^2},$$

where y_i is the measured or observed value for the output variable, in the $i-th$ observation, $\hat{y}_i$ is the estimated value of the same variable and n is the total number of observations. Finally, $\bar{y}$ is the mean value of the experimental values.

Root Mean Square Error. RMSE is a statistical measure of the difference between the values predicted by a model and the observed values. It is calculated as the square root of the mean of the squared differences between the predicted and observed values and it has its units.

$$\text{RMSE} = \sqrt{\frac{1}{n}\sum_{i=1}^{n}(y_i - \hat{y}_i)^2}$$

Mean Absolute Error. It represents the average absolute difference between predicted and actual values.

$$\text{MAE} = \frac{1}{n}\sum_{i=1}^{n}|y_i - \hat{y}_i|$$

Mean Absolute Percentage Error. As the MAE, it calculates the difference between the predicted and the actual values, but in this case it does so in relative terms:

$$\text{MAPE} = \frac{1}{n}\sum_{i=1}^{n}\left|\frac{y_i - \hat{y}_i}{y_i}\right| \times 100\%$$

5.2 First principle modelling

5.3 Data-driven modelling

Machine learning algorithms are unique in their ability to obtain models and extract patterns from data, without being explicitly programmed to do so. They are more effective with large volumes of data but can also be applied to build steady state regression models with less information of a process.

5.3.1 Gaussian Process Regression

5.3.2 Artificial Neural networks

Artificial Neural Networks (ANNs), as the name suggests, have a behavior similar to biological neurons. Their structure is formed by a succession of layers, each one composed by nodes (or neurons) and they receive as input the output of the previous layer. This process is subsequently repeated until the final layer which has a number of neurons equal to the number of outputs.

There are important aspects to be considered in the ANN model design, such as the model configuration, the network architecture and the network topology. They are discussed below.

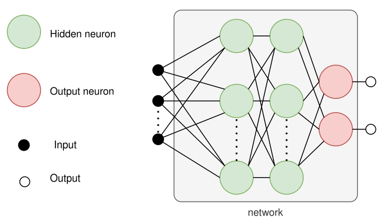

(a) MIMO configuration

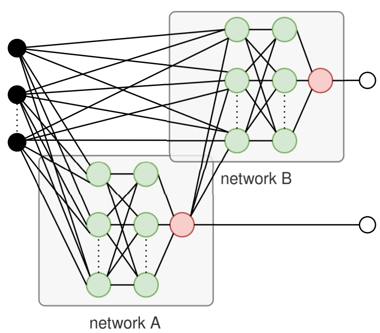

(b) Cascade configuration

Figure 5.1: ANN model configurations

Model configuration. If the model has more than one output, several configurations are available for the implementation of the model as shown in Figure 11.2. The first one is a Multiple Inputs Multiple Outputs (MIMO) configuration, where a single network receives all the inputs and directly produces all predicted outputs. The second one is a cascade structure. This cascading approach involves training a network (*network A* in Figure 11.2 (b)) to predict one output using the available inputs. Subsequently, these inputs, along with the output from the first-output-predicting network, are fed into a second network (*network B* in Figure 11.2 (b)) that is in charge of forecasting the second output. This procedure can be repeated as many times as desired. A potential advantage of this configuration is that it may reduce the experimental data requirements to obtain satisfactory results. A third option is the combination of both configurations, where some networks may predict several outputs, while others are fed some of these outputs as subsequently use them as inputs.

Network architectures. Three network architectures have been implemented and tested:

1. Feed Forward (FF) network - Figure 5.2 (a). This is the base network architecture, where different layers are added sequentially and the flow of information is unidirectional. The transfer function adopted in the hidden layers is the differentiable *Log-Sigmoid*[1], whereas the one employed in the output layer is a linear one with no saturations.
2. Cascade-forward (CF) network - Figure 5.2 (b). It is a variation on the feedforward network since it adds direct connections from the input and hidden layers to the output layer.
3. Radial Basis Function (RBF) network - Figure 5.2 (c). The transfer functions used in the first layer of the RBF network are different, they are local Gaussian like functions. Also, instead of multiplying by the weights, the distance between inputs and weights is computed and the bias is multiplied instead of added [12].

1: Defined as $logsig(x) = 1/(1+e^{-x})$, mapping any real input to a value between 0 and 1.

[12]: Hagan et al. (2014), *Neural Network Design*

Network topology. Two-layer networks (one hidden and one output layer) can learn almost any input-output relationship, including non-linear ones. Adding more layers can improve the learning for more complex problems. However, increasing the number of layers or neurons per layer increases the training computational requirements, requires more data for a satisfactory model and can lead to overfitting. Therefore, the process is usually started with two layers and then the number of layers is increased if they do not perform satisfactorily [12]. In this study, for the feedforward and cascade-forward architectures, one and two hidden layers have been tested with the following configurations: 5, 10, 20, 5-5, 5-10, 10-5, 10-10. For the case of the RBF, it only has one hidden layer and

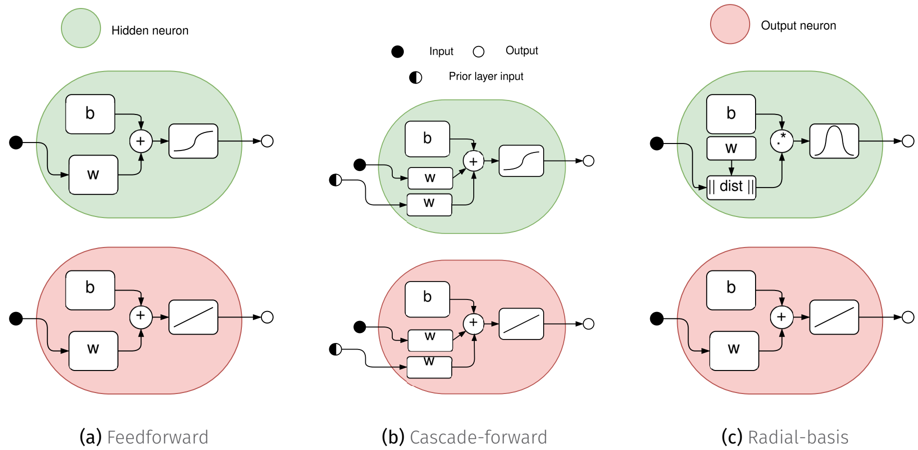

Figure 5.2: Considered ANN architectures

neurons are added sequentially during the training process up to a maximum which is set to 120 neurons.

Training process. The next important aspect to consider is the training process. For the FF and CF networks many Gradient- or Jacobian-based algorithms can be utilized. In this case, the Levenberg-Marquardt backpropagation algorithm [13] has been used. It is a fast algorithm, ideal for multilayer networks with up to a few hundred weights and biases enabling efficient training. The training in this case is done in batches since sequential training is slower and does not produce better results. All data have been normalized applying the z-score normalization method. The criteria established for deciding when to stop the training is the following one: when the performance on the validation set increases (worsens) or when the gradient is below a minimum (1×10^{-7}) for a number of iterations or epochs, or when a maximum number of 1000 epochs is reached. The number of iterations to wait, often refereed as patience, is set to 6. Finally, the selected network parameters will be those of the best epoch.

[13]: Beale et al. (2010), "Neural Network Toolbox"

For each network architecture, the training process was repeated a total of ten times (this is the recommended practice if the computational requirements allow it, since it guarantees reaching a global optimum with a high degree of confidence [14]). The optimal architecture and training was selected according to a performance function, which in this case has been the Mean Squared Error (MSE) with the values normalized.

[14]: Hamm et al. (2007), "Comparison of Stochastic Global Optimization Methods to Estimate Neural Network Weights"

In the case of the RBF network, the chosen training method consists in two stages which treats the two layers of the RBF network separately. The first layer weights and biases are tuned based on the orthogonal least squares method [12], while for the second layer are computed in one step using a linear least-squares algorithm. During training, neurons are added to the first layer (in increments of 20) trying to minimize the MSE to some goal, which in this case is set depending on the case study: 10 for the MIMO configuration and 0 ($°C^2$) and 20 (l^2/h^2) for temperature and water lost networks, respectively, for the cascade configuration. Finally, a parameter called spread is used to set the first layer biases. Larger values of this parameter promote a smoother approximation of the training data (more generalization), conversely, lower values provide a more exact fit to the training data. Values from 0.1 to 30 have been tested for this parameter.

[12]: Hagan et al. (2014), *Neural Network Design*

5.3.3 Random Forest

5.3.4 Gradient Boosting

5.4 Hybrid modelling

5.5 Data-driven from first-principles models. Sample generation

One important advantage that first-principles models have over data-driven is their scalability, that is, the ability to adapt a model developed and validated in a pilot-scale system, to a large scale one. This is true for many systems as long as the system configuration remains the same. This allows to study and analyze pilot scale plants and extrapolate the results to industrial sized plants. In addition, these type of model are also capable of predicting the behaviour of the modelled systems in conditions that have not been tested (*e.g.* different operating or environmental conditions), although the reliability of the model could be lower if these conditions move away from those experimentally used for some parameter calibration.

On the contrary, data-driven models are very specific to the system and operating ranges they are trained for. That is why training/calibrating a data-driven model with data from a first-principles model is a common practice to obtain a model that can be used in a larger range of operating conditions...

The process of generating samples from a first-principles model to train a data-driven model is called sample generation. It consists of running the first-principles model for a set of input parameters, which can be selected randomly or following a specific distribution, and then using the outputs of the first-principles model as the training data for the data-driven model.

The first step is to define the input parameters and their ranges. This can be done by selecting the most relevant parameters for the system and determining their ranges based on the system's operating conditions. The next step is to generate a set of input parameters, which can be done using different methods such as Latin Hypercube Sampling, Monte Carlo Sampling, Sobol Sampling, or simply grid sampling. These methods allow to generate a set of input parameters that cover the entire range of the input parameters and ensure that the generated samples are representative of the system's behaviour. Once the input parameters are defined, the first-principles model is run for each set of input parameters, and the outputs of the model are recorded. Finally, the recorded outputs are used to train the data-driven model.

6 Sensitivity analysis

It involves systematically assessing how variations in input parameters impact the model's outputs. In this case, the Sobol method [15], which is a variance-based approach, has been used. This method decomposes the total variance of the model output into contributions from individual input parameters and their interactions. By quantifying the relative importance of each parameter, Sobol analysis facilitates the identification of influential factors, enabling a more nuanced understanding of complex systems characterized by numerous interacting variables.

[15]: Nossent et al. (2011), "Sobol'sensitivity Analysis of a Complex Environmental Model"

The analysis results are different sensitivities indices such as total sensitivity indices (total-order), first-order sensitivity indices (first-order), and interaction sensitivity indices (second-order). First-order measures the direct effect of an input variable on the output, excluding interaction effects with other variables, while the second-order measures specifically this interaction effects. Finally, total-order indices account for the total effect of an input variable, including both direct and interaction effects.

6.1 Sensitivity analysis as a model analysis tool

Sobol sensitivity analysis provides a quantitative basis for assessing the consistency and validity of results when different approaches to model a system are compared. ANNs models with similar sensitivity analysis outcomes to those of the physical model, are likely to capture the essential features of the system, offering a means to verify their credibility and ensuring that the proposed solutions align with the underlying physical principles. Therefore, Sobol sensitivity analysis emerges as a powerful tool not only for understanding the system input-outputs relationships, but also as a way to validate and compare various modelling approaches. The sensitivity analysis has been performed using *SAlib*, an open source sensitivity analysis tool for the *Python* programming language [16, 17].

[16]: Herman et al. (2017), "SALib: An Open-Source Python Library for Sensitivity Analysis"

[17]: Iwanaga et al. (2022), "Toward SALib 2.0: Advancing the Accessibility and Interpretability of Global Sensitivity Analyses"

6.2 Sensitivity analysis as a measurement influence quantification tool

Sensitivity analysis can also be used to quantify the influence of measurement...

Control overview 7

asdad

7.1 PID controllers

7.2 Hierarchical control

8 Optimization overview

A general expression to define an optimization problem is:

$$\min_{\mathbf{x},\mathbf{e};\theta} \quad J = f(\mathbf{x},\mathbf{e};\theta) \quad \text{s.t.} \quad g_i(\mathbf{x}) \leq 0, \quad i = 1,\dots,m \tag{8.1}$$

where $\mathbf{x}$ is the vector of decision variables, $f(\mathbf{x})$ is the objective function to be minimized, and $g_i(\mathbf{x})$ are the constraints of the problem. The objective function is a scalar function that maps the decision variables to a real number, representing the cost or performance of the system. The constraints are functions that restrict the feasible region of the problem, defining the set of values that the decision variables can take. The optimization problem is to find the values of the decision variables that minimize the objective function while satisfying the constraints.

Regarding the constraints, they can be categorized in two types depending whether they can be evaluated before evaluating the objective function or not.:

- **Bounds**. These are constraints that limit the range of the decision variables, such as

  $$x_i \in [l_i, u_i], \quad i = 1,\dots,n$$

  where l_i and u_i are the lower and upper bounds of the decision variable x_i, respectively[1].
- **Constraints**. These are constraints that restrict the feasible region of the problem, such as

  $$g_i(\mathbf{x}) \leq 0, \quad i = 1,\dots,m$$

  where $g_i(\mathbf{x})$ are the constraint functions that depend on the decision variables $\mathbf{x}$, and m is the number of constraints. They can only be known after evaluating the objective function.

1: Also known as box-bounds

8.1 NLP problems

Non-Linear Programming (NLP)

8.2 MINLP problems

Mixed Integer Non-Linear Programming (MINLP)

8.3 Multi-objective optimization

8.4 Optimization algorithms

9 Research plan

asdad

9.1 Hypothesis

9.2 Objectives

10 Contributions

asdad

Optimal water and electricity management in a combined cooling system

TL;DR

In the pursuit of extending the use and feasibility of solar thermal applications, a case study consisting of a commercial 50 MW-8 hours of storage CSP plant, Andasol-II, is analyzed in annual simulations where the cooling solution makes use of the novel proposed Combined Cooling System (CCS). To obtain these results, a model of the CCS has been developed based on the same configuration as the PSA pilot plant. Different optimization strategies based on evolutionary algorithms have been implemented to adapt the system operation to the changing conditions. The strategy has been experimentally validated in the pilot plant and the simulated results show than the proposed scheme can yield ... compared to the DC only and ... with the WCT only alternatives.

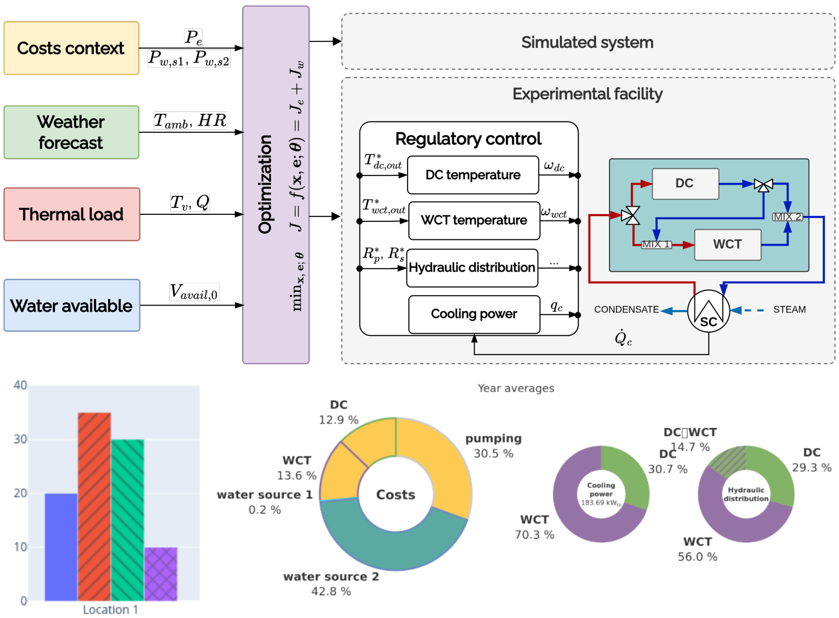

(a) Andasol-II CSP plant case study results

Figure 10.1: Results for the analyzed case study in this part. The first bar plot compares the specific cost of the different cooling alternatives (lower is better). The second pie chart shows the breakdown of the costs, and the third and fourth pie charts show the cooling power distribution between DC and WCT and

In pie chart, rename pumping to recirculation. Q to $\dot{Q}$

Derived scientific contributions

Structure

This part is structured as follows: in the first two chapters the methodology is described, specifically the modelling in (Chapter ?? (??)) is presented for the CCS, and the optimization framework in Chapter 12 (Optimization of a combined cooling system). The third chapter presents the experimental facility (Chapter 13 (Combined cooling pilot plant at Plataforma Solar de Almería)) that is used to experimentally validate the model and the optimization strategy integrated in a hierarchical control scheme in Chapter 14 (Validation in the combined cooling pilot plant). The final chapter, Chapter 15 (Annual analysis: ANDASOL-II CSP plant), describes and analyzes the results of the annual simulations performed for the Andasol-II CSP plant.

Modelling of a combined cooling system 11

TL;DR

This chapter describes the steady-state modelling of the different components of a combined cooling system, mainly a WCT and a DC. Different alternatives are presented: from physical models to data-driven approaches, including the generation of samples for data-driven models trained using data from a physical model. Models are also developed for the other components of the system and finally it is shown how they are integrated into a complete system model. The complete system model interface is defined at Model **??** and a block diagram is presented in Figure 11.3 including all relevant variables.

Introduction

In order to study the potential advantages of making use of a combined cooling system, it is first necessary to develop the modelling of its components. Since the objective is performance prediction, this chapter focuses on the steady state modelling of the combined cooler main components, *i.e.* the WCT and the DC. More specifically, the aim is to compare two modelling strategies: that based on physical equations (Section 5.2) and that based on black box models (Section 5.3) such as ANNs, in order to see which one is more suitable for its integration in the optimization of the complete process.

Ahora mismo esta introducción es demasiado parecida al TL;DR, hay que distinguirla

This chapter presents a comparison between the two modelling approaches, at steady state and with a focus on optimization applications, in terms of predictive capabilities, experimental and instrumentation requirements, execution time, implementation and scalability. A sensitivity analysis is performed to further analyze and compare each case study. It also presents and evaluates all relevant aspects of interest in the development of such models, specifically for ANNs, model configuration, architecture and topology are discussed. Other system components are also described in Section 11.3 (Other components) and finally their integration is discussed in Section 11.4 (Complete system).

11.1 Wet cooler

In the case of the models based on physical equations, the analysis of wet cooling towers has its origin in [18], in which the theory for their performance evaluation was developed. Merkel proposed a model based on several assumptions to simplify the heat and mass transfer equations to a simple hand calculation. However, these assumptions mean that Merkel's method does not reliably represent the physics of the heat and mass transfer process in a cooling tower. This was already stated by Bourillot [19] who concluded that the Merkel method is simple to use and can correctly predict cold water temperature when an appropriate value of the coefficient of evaporation is used. However, it is insufficient for the estimation of the characteristics of the warm air leaving the fill and for the calculation of changes in the water flow rate due to evaporation. Jaber and Webb [20] developed the equations necessary to apply the effectiveness-NTU[1] method directly to counterflow or crossflow cooling towers. This approach is particularly useful in the latter case and simpler compared to a more conventional numerical procedure. Notice that the effectiveness-NTU

[18]: Merkel (1925), "Verdunstungskühlung"

[19]: Bourillot (1983), "Hypotheses of Calculation of the Water Flow Rate Evaporated in a Wet Cooling Tower"

[20]: Jaber et al. (1989), "Design of Cooling Towers by the Effectiveness-NTU Method"

1: The effectiveness-NTU method estimates how well a heat exchanger transfers heat by comparing the actual heat transfer to the maximum possible, using a parameter, Number of Transfer Units (NTU), that reflects its size and flow characteristics.

method is based on the same simplifying assumptions as the Merkel method. On the other hand, Poppe and Rögener [21] developed the Poppe method. They derived the governing equations for heat and mass transfer in a wet cooling tower and did not make any simplifying assumptions as in the Merkel theory, which makes it a very precise model. As a matter of fact, predictions from the Poppe formulation have resulted in values of evaporated water flow rate that are in good agreement with full scale cooling tower test results [22]. This model has already been used for the evaluation of the thermal performance of solar power plants using different condensation systems (wet, dry and hybrid system), as can be found in Cutillas et al. [23].

[21]: Poppe et al. (1991), "Berechnung von Rückkühlwerken"

[22]: Kloppers et al. (2005), "A Critical Investigation into the Heat and Mass Transfer Analysis of Counterflow Wet-Cooling Towers"

[23]: Cutillas et al. (2021), "Energetic, Exergetic and Environmental (3E) Analyses of Different Cooling Technologies (Wet, Dry and Hybrid) in a CSP Thermal Power Plant"

In the case of black box models, numerous authors in the literature have designed ANN models for WCT with different objectives, such as performance prediction, simulation and optimization. One of the first works in this area is the one described in [24] where an ANN model was developed to predict the performance of a forced-counter flow cooling tower at lab scale. In this case, the input variables were the dry bulb temperature, the relative humidity of the air stream entering the tower, the temperature of the water entering the tower, the air volume flow rate and the cooling water mass flow rate. The outputs of this model were the heat rejection rate at the tower, the mass flow rate of water evaporated, the temperature of the cooling water at the tower outlet, the dry bulb temperature and the relative humidity of the air at the outlet of the tower. The results obtained with a 5-5-5[2] ANN demonstrated that wet cooling towers at lab-scale can be modelled using ANNs with a high degree of accuracy. There are also ANN models for Natural Draft Counter-flow Wet Cooling Towers (NDWCT) at lab-scale, such as the one proposed by [25]. In this case, the authors used a 4-8-6 ANN structure and considered some additional variables, such as air gravity, wind velocity, heat transfer coefficients and efficiency as outputs. All these works can be useful to validate the model development methodology but may fail predicting the performance of WCT at larger scale. In this sense, special attention deserves the study carried out by [26] where an 8-14-2 ANN model was proposed to predict the performance (the cooling number and the evaporative loss proportion) of NDWCTs at commercial scale. The model is based on 638 sets of field experimental data collected from 36 diverse NDWCTs used in power plants. It is a very challenging work since it covers samples from a wide range of tower sizes and capacities being the Mean Relative Error (MRE) below 5 %.

[24]: Hosoz et al. (2007), "Performance Prediction of a Cooling Tower Using Artificial Neural Network"

2: The notation n_1-...-n_l represents the architecture of the ANN model, where l is the number of layers and n_i are the nodes in each one of the layers.

[25]: Gao et al. (2013), "Artificial Neural Network Model Research on Effects of Cross-Wind to Performance Parameters of Wet Cooling Tower Based on Level Froude Number"

[26]: Song et al. (2021), "A Novel Approach for Energy Efficiency Prediction of Various Natural Draft Wet Cooling Towers Using ANN"

From the literature review, it can be stated that there are works based on Poppe and ANN models that evaluate the main output variables of WCTs. Nevertheless, to the author knowledge, there are no studies focused on the comparison between both modelling strategies. Also lacking is a comprehensive analysis of the different aspects that affect the models development and performance.

The static models presented in this section have been developed to predict two main outputs, the water temperature at the outlet of the WCT, $T_{w,o}$, and the water consumed due to evaporation losses, $\dot{m}_{w,lost}$. The inputs variables required by both modelling approaches, Poppe model and ANN models, are: the cooling water flow rate ($\dot{m}_w$), the water temperature at the inlet of the WCT ($T_{w,i}$), the ambient temperature (T_∞), the ambient relative humidity (ϕ_∞) and the frequency percentage of the fan (f_{fan}) (or its equivalence in air mass flow rate[3], $\dot{m}_a$).

3: ANN uses as input f_{fan} whereas Poppe's model uses $\dot{m}_a$.

11.1.1 Poppe model

The well-known Merkel number is accepted as the performance coefficient of a wet cooling tower [27]. This dimensionless number is defined in Equation 11.1, and it measures the degree of difficulty of the mass transfer processes occurring in the exchange area of a wet cooling tower.

[27]: Navarro et al. (2022), "Critical Evaluation of the Thermal Performance Analysis of a New Cooling Tower Prototype"

$$Me = \frac{h_D a_v V}{\dot{m}_w}, \tag{11.1}$$

where h_D is the mass transfer coefficient, a_V is the surface area of exchange per unit of volume and V is the volume of the transfer region.

The Merkel number can be calculated using the Merkel and Poppe theories for the performance evaluation of cooling towers. On the one hand, the Merkel theory [18] relies on several critical assumptions, such as the Lewis factor (Le) being equal to 1, the air exiting the tower being saturated with water vapour and it neglects the reduction of water flow rate by evaporation in the energy balance. On the other hand, the Poppe theory [21], which is the one used in this work, do not consider simplifying assumptions, thus being the one most usually preferred. In this theory, the authors derived the governing equations for heat and mass transfer in the transfer region of the wet cooling tower (control volume shown in Figure 11.1) assuming a one dimensional problem. In this figure, the red and green dashed lines indicate the fill and air-side control volumes, respectively.

[18]: Merkel (1925), "Verdunstungskühlung"

[21]: Poppe et al. (1991), "Berechnung von Rückkühlwerken"

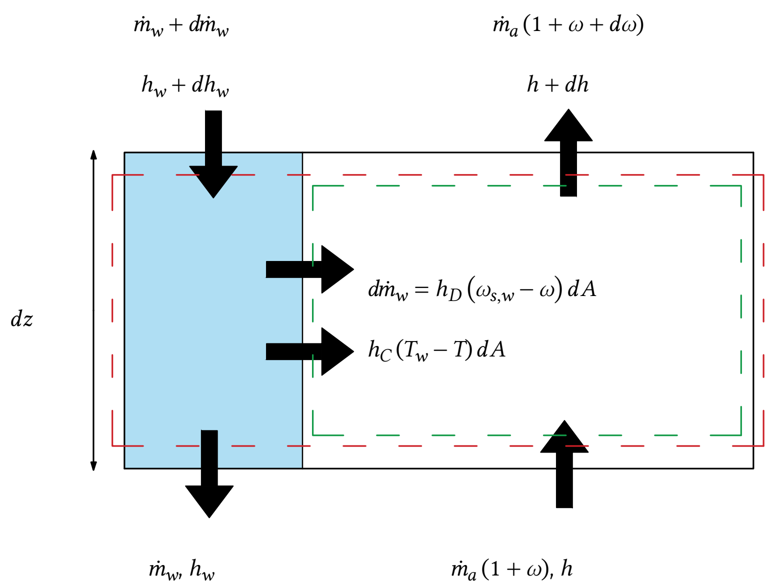

Figure 11.1: Control volume in the exchange area of a wet cooling tower arrangement.

Following the detailed derivation process and simplification of the previously-mentioned governing equations described in [27], the major following equations for the heat and mass transfer obtained, according to the Poppe theory, are:

$$\frac{d\omega}{dT_w} = \frac{c_{p_w}\frac{\dot{m}_w}{\dot{m}_a}(\omega_{s,w}-\omega)}{(h_{s,w}-h)+(\mathrm{Le}-1)\left[(h_{s,w}-h)-(\omega_{s,w}-\omega)h_v\right]-(\omega_{s,w}-\omega)h_w} \tag{11.2}$$

$$\frac{dh}{dT_w} = c_{p_w}\frac{\dot{m}_w}{\dot{m}_a}\left[1+\frac{(\omega_{s,w}-\omega)c_{p_w}T_w}{(h_{s,w}-h)+(\mathrm{Le}-1)\left[(h_{s,w}-h)-(\omega_{s,w}-\omega)h_v\right]-(\omega_{s,w}-\omega)h_w}\right] \tag{11.3}$$

$$\frac{d\mathrm{Me}}{dT_w} = \frac{c_{p_w}}{(h_{s,w}-h)+(\mathrm{Le}-1)\left[(h_{s,w}-h)-(\omega_{s,w}-\omega)h_v\right]-(\omega_{s,w}-\omega)h_w}, \tag{11.4}$$

where the quantity referred to as Me in Eq. 11.4, is the Merkel number calculated according to the Poppe theory. The above described governing equations can be solved by the fourth order Runge-Kutta method to provide the evolution of the air humidity ratio, air enthalpy and Merkel number inside the transfer area of the cooling tower (fill). Once these profiles are known, the amount of water lost due evaporation can be calculated as per Eq. Equation 11.6. Refer to [27] for additional information concerning the calculation procedure.

[27]: Navarro et al. (2022), "Critical Evaluation of the Thermal Performance Analysis of a New Cooling Tower Prototype"

$$Me = \frac{h_D a_v V}{\dot{m}_w}, \tag{11.5}$$

$$\dot{m}_{w,lost} = \dot{m}_a(\omega_{a,o} - \omega_{a,i}) \tag{11.6}$$

It is important to mention that the Merkel number varies with the operation conditions and its value can be obtained using a correlation with the water-to-air mass flow ratio as an independent variable. One of the proposed correlations in ASHRAE [28] is:

[28]: Ashrae (2004), "HVAC Systems and Equipment"

$$\mathrm{Me} = c\,(\dot{m}_w/\dot{m}_a)^{-n} \tag{11.7}$$

where the constants c and n can be obtained from the fitting of experimental data[4].

4: See Section 14.1.1 (Wet cooler model alternatives comparison and validation)

11.1.2 Samples generation for first-principles to data-driven models

The first pair of input variables for the WCT sample generation are the wet bulb temperature (T_{wb}) and the difference between this temperature and the system inlet temperature (ΔT_{wb-in}). The wet bulb temperature is used instead of the ambient temperature or the relative humidity, because as it can be derived from the physical model, it is the most relevant thermodynamic variable for the wet cooling tower performance. Using both the ambient temperature and the relative humidity would lead to a larger than necessary input space with many duplicate samples, as the wet bulb temperature is a function of both variables. The second pair of input variables are the cooling water flow rate (q_{wct}) and, following the reasoning from the physical model, the air to water mass flow ratio ($\dot{m}_a/\dot{m}_{wct}$), since it is a key parameter in defining the operating conditions of the tower. From the resulting 2D grid, valid combinations are obtained by calculating the air mass flow rate and finding if a valid fan speed can be obtained using an air mass flow rate to fan speed empirical correlation.

Finally, all valid thermodynamic and operational combinations are merged into a comprehensive sample set, enabling detailed system evaluations across a realistic and constrained input space.

11.1.3 Model interface

Model 11.1: Wet cooling tower

$$T_{wct,out},\ C_{w,wct} = \text{wct model}(q_{wct},\ \omega_{wct},\ T_{amb},\ HR,\ T_{wct,in})$$

Model 11.2: Wet cooling system model

$$
\begin{aligned}
T_{wct,out}, C_e, C_w, T_{c,in}, T_{c,out} &= \text{wcs model}(q_{wct}, \omega_{wct}, T_{amb}, HR, T_{wct,in})\\
T_{c,in}, T_{c,out} &= \text{condenser model}(q_c, \dot{m}_v, T_v)\\
T_{wct,out}, C_{w,wct} &= \text{wct model}(q_{wct}, \omega_{wct}, T_{amb}, HR, T_{c,out})\\
C_{e,c} &= \text{electrical consumption}(q_c)\\
C_{e,wct} &= \text{electrical consumption}(\omega_{wct})\\
C_e &= C_{e,wct} + C_{e,c}\\
C_w &= C_{w,wct}
\end{aligned}
$$

11.2 Dry cooler

11.2.1 Physical model

a

Pendiente de basarse en el artículo del modelo físico del DC con Elxe

11.2.2 Samples generation for first-principles to data-driven models

Similar to the wet cooling tower case, setting absolute values for both the inlet temperature and the environment temperature will lead to many unfeasible combinations ($T_{dc,in} \leq T_{db}$). So instead, values are generated for the temperature difference, therefore, a 2D grid is constructed using combinations of ambient/dry-bulb temperature (T_{amb}) and the difference between inlet and ambient temperature ((ΔT_{amb-in})). For each valid temperature pair (T_{amb}, $T_{dc,in}$), additional independent variables (q_{dc}, ω_{dc}) are combined via a Cartesian product, resulting in a full multidimensional grid of plausible operating points. This systematic procedure ensures a dense and uniform sampling across all relevant input dimensions. Finally, infeasible combinations are filtered based on physical constraints.

11.2.3 Model interface

Model 11.3: Dry cooler

$$T_{dc,out} = \text{dc model}(q_{dc}, \omega_{\text{dc}}, T_{\text{amb}}, T_{dc,in})$$

Model 11.4: Dry cooling system model

$$
\begin{aligned}
T_{dc,out}, C_e, T_{c,in}, T_{c,out} &= \text{dcs model}(q_{dc}, \omega_{dc}, T_{amb}, T_{dc,in}) \\
T_{c,in}, T_{c,out} &= \text{condenser model}(q_c, \dot{m}_v, T_v) \\
T_{dc,out} &= \text{dc model}(q_{dc}, \omega_{\text{dc}}, T_{\text{amb}}, T_{c,out}) \\
C_{e,c} &= \text{electrical consumption}(q_c) \\
C_{e,dc} &= \text{electrical consumption}(\omega_{dc}) \\
C_e &= C_{e,dc} + C_{e,c}
\end{aligned}
$$

11.3 Other components

11.3.1 Electrical consumption

Electrical consumption is modelled with polynomial regressions of order 3 from experimental data:

Model 11.5: Electrical consumption

$$
\begin{aligned}
C_e &= \text{electrical consumption model}(x) \\
C_e &= p_1 \cdot x^3 + p_2 \cdot x^2 + p_3 \cdot x + p_4
\end{aligned}
$$

where C_e represents the electrical consumption, and x is the input variable (e.g., the recirculated cooling water flow rate, particular cooler fan speed, etc.). The coefficients p_i correspond to a polynomial regression and must be calibrated individually for each component.

11.3.2 Surface condenser

The surface condenser is a heat exchanger that condenses steam into water, assuming that all the vapor that enters the condenser (at saturated conditions), leaves it as saturated liquid, it can be modelled by applying the first law of thermodynamics, which states that the heat lost by the steam (*released*) is equal to the heat gained by the cooling water (*absorbed*), and equal to the heat transferred by the condenser heat transfer surfaces (*transferred*).

Model 11.6: Surface condenser

$$
\begin{aligned}
T_{c,in}, T_{c,out} &= \text{condenser model}(\dot{m}_c, T_v, \dot{m}_v)\\
LMTD &= \frac{T_{c,out} - T_{c,in}}{\ln\left(\frac{T_v - T_{c,in}}{T_v - T_{c,out}}\right)}\\
\dot{Q}_{released} &= \dot{m}_v \cdot (h_{sat.vap} - h_{sat.liq})\\
\dot{Q}_{absorbed} &= \dot{m}_c \cdot c_p(T_{c,out} - T_{c,in})\\
\dot{Q}_{transferred} &= U \cdot A \cdot LMTD\\
U &= \ldots
\end{aligned}
$$

The condenser area (A) is a constant parameter

where $T_{c,in}$ and $T_{c,out}$ are the cooling water inlet and outlet temperatures, respectively, $\dot{m}_c$ the cooling water mass flow rate, T_v vapour temperature and $\dot{m}_v$ its mass flow rate and $h_{sat,vap}$ and $h_{sat,liq}$ are the specific enthalpies of the steam at the inlet and outlet of the condenser, respectively. $\dot{Q}$ represents the heat transfer rate *i.e.* the thermal power.

11.3.3 Mixers

The mixers outlet flow ($q_{mix,out,i}$) and temperature ($T_{mix,out,i}$) can be determined with a simple mass and energy balances from its inlets streams ($q_{mix,in}$, $T_{mix,in}$):

Model 11.7: Mixer model

$$q_{mix,out}, T_{mix,out} = \text{mixer model}(q_{mix,in,1}, T_{mix,in,1}, q_{mix,in,2}, T_{mix,in,2}) \tag{11.8}$$

$$q_{mix,out} = q_{mix,in,1} + q_{mix,in,2} \tag{11.9}$$

$$
\begin{aligned}
T_{mix,out} = T_{mix,in,1} \cdot \frac{c_p(T_{mix,in,1})}{c_p(T_{out,i})} \frac{q_{mix,in,1}}{q_{mix,out,i}} +\\
T_{mix,in,2} \cdot \frac{c_p(T_{mix,in,2})}{c_p(T_{out,i})} \frac{q_{mix,in,2}}{q_{mix,out,i}}
\end{aligned} \tag{11.10}
$$

where $c_p(\cdot)$ is the specific heat, which can be assumed to be the same for the mixing temperature differences of this type of system.

11.4 Complete system

The complete model of the combined cooling system integrates the models of the WCT and DC, along with the surface condenser and the mixers, as defined in Model 11.8 (Complete system)[5]. The full diagram, including all variables, is shown in Figure 11.3.

5: Although the electrical consumption for cooling water recirculation is attributed to the condenser in this model, other components—particularly the hydraulic circuit and the dry cooler—also contribute significantly to circulation resistance

To solve the system, the condenser model is evaluated first, providing the inlet temperature for the dry cooler. Once the dry cooler is solved, the resulting temperatures allow for solving the wet cooling tower. Finally, the mixers are evaluated to determine the final outlet temperature of the combined cooler, which should match the condenser's inlet temperature.

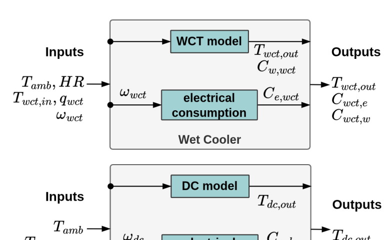

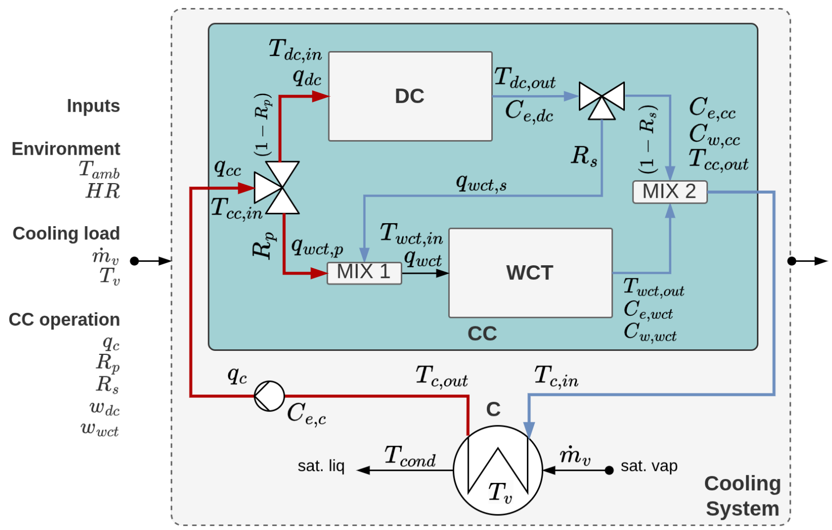

Figure 11.3: Complete model diagram of the combined cooling system

Model 11.8: Combined cooling system

$$T_{cc,out}, C_e, C_w, T_{c,in}, T_{c,out} = \text{ccs model}(q_c, R_p, R_s, \omega_{dc}, \omega_{wct}, T_{amb}, HR_i, T_v, \dot{m}_v)$$

$$T_{cc,in} = T_{c,out}$$

$$T_{dc,in} = T_{cc,in}$$

$$q_{dc} = q_c \cdot (1 - R_p)$$

$$q_{wct,p} = q_c \cdot R_p$$

$$q_{wct,s} = q_{dc} \cdot R_s$$

$$T_{dc,out}, C_{e,dc} = \text{dc model}(q_{dc}, \omega_{\text{dc}}, T_{\text{amb}}, T_{dc,in})$$

$$q_{wct}, T_{wct,in} = \text{mixer model}(q_{wct,p}, T_{Tcc,in}, q_{wct,s}, T_{dc,out})$$

$$T_{wct,out}, C_{e,wct}, C_{w,wct} = \text{wct model}(q_{wct}, \omega_{wct}, T_{amb}, HR, T_{wct,in})$$

$$T_{c,in}, T_{c,out} = \text{condenser model}(q_c, \dot{m}_v, T_v)$$

$$q_{cc}, T_{cc,out} = \text{mixer model}(q_{wct}, T_{wct,out}, q_{dc}, T_{dc,out})$$

$$C_{e,c} = \text{electrical consumption}(q_c)$$

$$C_{e,dc} = \text{electrical consumption}(\omega_{dc})$$

$$C_{e,wct} = \text{electrical consumption}(\omega_{wct})$$

$$C_e = C_{e,dc} + C_{e,wct} + C_{e,c}$$

$$C_w = C_{w,wct}$$

12 Optimization of a combined cooling system

TL;DR

This chapter describes optimization problems for a combined cooling system, a DC and a WCT as well as different optimization strategies propositions to solve them. The objective is to minimize the daily cost of operation made up by the electricity and water costs, while ensuring the cooling demand is met. They key challenge is to manage the available water resource, since there is a limited amount of cheap rainwater available and any excess water required must be purchased at a significantly higher cost. From the alternatives, this can only be effectively achieved by the shrinking horizon optimization strategy applied to the combined cooler for which an implementation methodology is proposed.

Introduction

From a literature review, works can be found that optimize the operation of the cooling system. Of special interest are the works of Marín [29, 30] where a .... strategy is proposed to optimize both the power block and the cooling system. In [29] a WCT is analyzed, while on [30] a DC is used instead. Annual analysis is performed (sampled monthly) and a techno-economic analysis is performed. The results show ... It can be concluded that there are not many works focusing on the operation optimization. From those that do, they study only one particular system, either a dry cooler or a wet cooler, and not the combined cooling system. From those do, they are focused on the design optimization side, not on the operation.

El estado del arte está por terminar L

[29]: Martín et al. (2013), "Optimal Year-Round Operation of a Concentrated Solar Energy Plant in the South of Europe"

[30]: Martín (2015), "Optimal Annual Operation of the Dry Cooling System of a Concentrated Solar Energy Plant in the South of Spain"

In this chapter, the optimization of the operation of different cooling alternatives is analyzed in terms of their two main consumptions: electricity and water. The optimization problems are formulated to minimize the cost of cooling a thermal load, where this cost is made up by the two mentioned consumptions. Even though in principle this methodology could be applied to any application where cooling a thermal load is required, special focus is put on modelling and considering the water resource availability, since it is a key factor especially in solar thermal applications.[1]

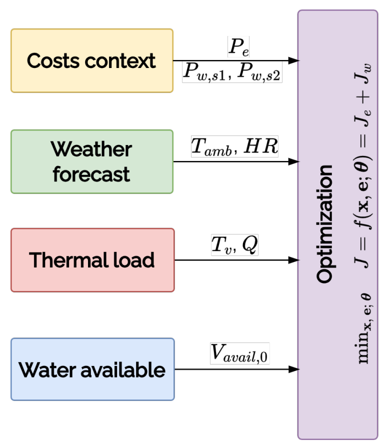

Figure 12.1: Block diagram of the optimization scheme including environment components

The chapter is structured as follows: first, the environment definition is presented in Section 12.1 (Environment definition), which includes a description of the variables taking part in the costs context, weather forecast, thermal load, and water resource availability. Next the two optimization strategies are presented, first a static optimization in Section 12.2 (Static optimization) where the dry cooler, wet cooler and combined cooler static problems are defined; followed by a shrinking horizon optimization approach in Section 12.3 (Horizon optimization) where the combined cooler is optimized over a prediction horizon. This last section includes a discussion on the problem nature and then presents the proposed methodology to solve it.

1: See Chapter 4 (Cooling overview)

12.1 Environment definition

The environment for the optimization problems described in this section includes the following components and is visualized in Figure 12.1:

Costs context The cooling system has mainly two associated operational costs: electricity (J_e) and water use (J_w). For the electricity the sale price of electricity (P_e) is used since whatever is consumed by the cooling system, it is electricity that cannot be sold to the market in the case of a system that produces electricity like a CSP plant, and it is electricity that needs to be purchased at market price in the case of any other system.
As for the water, two sources are considered, water price from source 1 is referred as $P_{w,s1}$ and $P_{w,s2}$ for source 2. Source 1 is cheaper than source 2.

Weather forecast The only two weather variables that have an impact on the cooling system are the ambient temperature (T_{amb}) and the relative humidity (HR) since they set the dry and wet bulb temperatures.

Thermal load The thermal load is defined either by a vapor flow rate ($\dot{m}_v$) or a thermal power ($\dot{Q}$), which enters the condenser at a temperature T_v.[2]

2: Vapor can also be referred as steam, usually steam is used when the vapor performs work, like in a turbine.

Water resource availability Two sources of water are available, one of them, the cheaper one coming from a dam is limited in volume (V_{avail}). The cheaper source (s_1) is prioritized until it is depleted, then the alternative source (s_2) is used:

$$C_{w,s1,i} = \frac{\min(V_{avail,i}, C_{w,i} \cdot T_s)}{T_s} \tag{12.1}$$

$$C_{w,s2,i} = C_{w,i} - C_{w,s1,i} \tag{12.2}$$

$$V_{avail,i} = V_{avail,i-1} - C_{w,s1,i} \cdot T_s \tag{12.3}$$

where i represents the step, at every step the amount used from each source is estimated and the source 1 availability is updated accordingly. C_w represents the flow rate of water consumed and T_s is the sample time at which steps are computed.

12.2 Static optimization

Static optimization problems are defined in a particular time, given an environment, and decisions do not take into account prior states or decisions, neither consider the effect on future state.

From a process perspective this also characterizes the cooling process, except for the water resource availability, being the only variable that depends on the previous state, *i.e.* is not static. Each time a static problem is evaluated, it begins with a specific initial water volume ($V_{\text{avail},0}$) for that step. After solving the problem, this volume must be updated before proceeding to the next step. As a result, evaluating multiple consecutive steps requires a sequential approach.

Reminder: Optimization problem definition

The general optimization function is defined as:[a]

$$\min_{\mathbf{x},\mathbf{e};\theta} \quad J = f(\mathbf{x}, \mathbf{e}; \theta) \quad \text{s.t.} \quad g_i(\mathbf{x}) \leq 0, \quad i = 1, \dots, m$$

where x is the decision vector, e represents the environment, and θ contains the fixed parameters.

[a] See Section ?? (??)

In order to streamline the problem formulation, a general combined cooling system model is used for every scenario. This unified model incorporates both the dry and wet coolers, as well as the shared surface condenser. For cases where only one cooler is used, the other can be effectively disabled by setting its associated variables to zero and configuring the hydraulic circuit to prevent water circulation through it.

12.2.1 Dry cooler

In the first case study, the optimization focuses exclusively on the dry cooler. Consequently, all variables and terms associated with the wet cooler, as well as water resource management, are omitted from the formulation, making the problem completely static[3]. This configuration is illustrated in Figure 12.2 and the problem is defined as follows:

3: Achieved by setting $R_p = 0$ and R_s=0

Problem: DC - static

$$\min_{\mathbf{x},\mathbf{e};\theta} \quad J = f(\mathbf{x}, \mathbf{e}; \theta) = C_e \cdot P_e$$

with:

$$T_{dc,out},\, C_e,\, T_{c,in},\, T_{c,out} = \text{dcs model}(q_c,\, \omega_{\text{dc}},\, T_{\text{amb}},\, T_v,\, \dot{m}_v)$$

- Decision variables
$$x = [q_c,\, \omega_{\text{dc}}]$$
- Environment variables
$$e = [T_{\text{amb}},\, P_e,\, T_v,\, \dot{m}_v]$$
- Fixed parameters
$$\theta = [R_p = 0,\ R_s = 0,\ \omega_{\text{wct}} = 0]$$

subject to:

- Box-bounds
  - $w_{dc} \in [\underline{w}_{dc}, \overline{w}_{dc}]$
  - $q_c \in [\underline{q}_c, \overline{q}_c]$
- Constraints
  - $|T_{\text{dc,out}} - T_{\text{c,in}}| \leq \epsilon_1$
  - $T_{\text{c,out}} \leq T_v - \Delta T_{\text{c-v,min}}$
  - $|Q_{\text{dc}} - Q_{\text{c,released}}| \leq \epsilon_2$

See Section ?? (??) for a detailed description of the dry cooler and Section 11.3.2 (Surface condenser) for the condenser model.

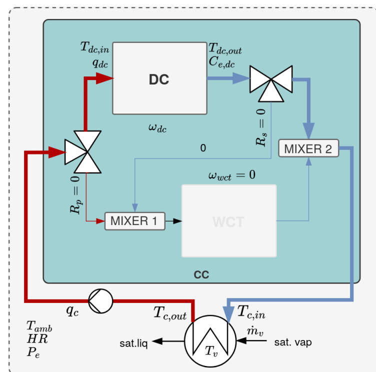

Figure 12.2: Diagram of the dry cooler only cooling problem

The cost of cooling (J) is equivalent to the cost of electricity (J_e), which in turn is the product of the electricity price (P_e) and the electricity consumption (C_e). Only two decision variables are defined, the cooling water recirculation flow rate (q_c) and the dry cooler fan speed (ω_{dc}). Any two pair of values for these variables that satisfy the bounds do not necessary yield a feasible solution, that is why three constrains are introduced, the first one ensures that the outlet cooler temperature matches the inlet condenser temperature (since they are directly connected, they must be the same), the second one ensures that the condenser outlet temperature respects the minimum temperature difference with the vapor temperature, and the last one ensures that the cooling duty of the dry cooler matches the one of the condenser.[4].

4: In order to better comprehend why mismatches between cooler and condenser can exist, the reader is referred to Section 11.4 (Complete system)

12.2.2 Wet cooler

Conversely to the dry cooler, the wet cooler optimization problem is configured by setting $R_p = 1$, effectively disabling the dry cooler. In this case, water associated variables are included in the problem formulation:[5]

5: See Section 11.1 (Wet cooler) for a detailed description of the wet cooler and condenser model.

Problem: WCT – static

$$\min_{\mathbf{x},\mathbf{e};\theta} \quad J = f(\mathbf{x}, \mathbf{e}; \theta) = J_e + J_w$$

with:

$$\begin{aligned} J_e &= C_e \cdot P_e \\ J_w &= C_{w,s1} \cdot P_{w,s1} + C_{w,s2} \cdot P_{w,s2} \\ C_{w,s1} &= \min\left((V_{avail}, C_w \cdot T_s)/T_s\right) \\ C_{w,s2} &= C_w - C_{w,s1} \\ T_{wct,out},\ C_e,\ C_w,\ T_{c,in},\ T_{c,out} &= \text{wcs model}(q_c, \omega_{wct}, T_{amb}, HR, T_v, \dot{m}_v) \end{aligned}$$

- Decision variables

$$x = [q_c,\ \omega_{\text{wct}}]$$

- Environment variables

$$e = [T_{\text{amb}}, HR,\ P_e,\ P_{w,s1},\ P_{w,s2}, V_{avail},\ T_v,\ \dot{m}_v]$$

- Fixed parameters

$$\theta = [R_p = 1,\ R_s = 0,\ \omega_{\text{dc}} = 0]$$

subject to:

- Box-bounds
  - $w_{wct} \in [\underline{w}_{wct}, \overline{w}_{wct}]$
  - $q_c \in [\underline{q}_c, \overline{q}_c]$
- Constraints
  - $|T_{\text{wct,out}} - T_{\text{c,in}}| \leq \epsilon_1$
  - $T_{\text{c,out}} \leq T_v - \Delta T_{\text{c-v,min}}$
  - $|Q_{\text{wct}} - Q_{\text{c,released}}| \leq \epsilon_2$

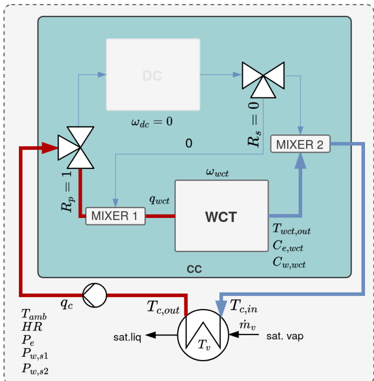

Figure 12.3: Diagram of the wet cooler only cooling problem

In this version of the problem, the decision vector is composed by the recirculation flow rate, but now the fan speed of the wet cooler (ω_{wct}) is included. The cost of cooling now includes the cost of water (J_w) and its availability is updated using the water consumption (C_w) as described in Equations (12.1)–(12.3). The environment now includes the air relative humidity and water prices.

12.2.3 Combined cooler

The last static optimization problem is the combined cooler, which incorporates both the dry and wet coolers, as well as the condenser. Here the hydraulic distribution is not fixed but is part of the decision variables, allowing the optimization to determine the optimal distribution between the two coolers. The problem is defined as follows:[6]

6: See Section 11.4 (Complete system) for a detailed description of the combined cooler and condenser model.

Problem: CC - static

$$\min_{\mathbf{x},\mathbf{e};\theta} \quad J = f(\mathbf{x}, \mathbf{e}; \theta) = J_e + J_w$$

with:

$$
\begin{aligned}
J_e &= C_e \cdot P_e \\
J_w &= C_{w,s1} \cdot P_{w,s1} + C_{w,s2} \cdot P_{w,s2} \\
C_{w,s1} &= \frac{\min(V_{avail}, C_w \cdot T_s)}{T_s} \\
C_{w,s2} &= C_w - C_{w,s1} \\
T_{cc,out}, C_e, C_w, T_{c,in}, T_{c,out} &= \text{ccs model}(q_c, R_p, R_s, \omega_{dc}, \omega_{wct}, T_{amb}, HR, T_v, \dot{m}_v)
\end{aligned}
$$

- Decision variables

$$x = [q_c, R_p, R_s, \omega_{\text{dc}}, \omega_{\text{wct}}]$$

- Environment variables

$$e = [T_{\text{amb}}, HR,\ P_e,\ P_{w,s1},\ P_{w,s2}, V_{avail},\ T_v,\ \dot{m}_v]$$

subject to:

- Box-bounds
  - $w_{dc} \in [\underline{w}_{dc}, \overline{w}_{dc}]$
  - $w_{wct} \in [\underline{w}_{wct}, \overline{w}_{wct}]$
  - $q_c \in [\underline{q}_c, \overline{q}_c]$
  - $R_p \in [0, 1]$
  - $R_s \in [0, 1]$
- Constraints
  - $|T_{\text{cc,out}} - T_{\text{c,in}}| \leq \epsilon_1$
  - $T_{\text{c,out}} \leq T_v - \Delta T_{\text{c-v,min}}$
  - $|Q_{\text{cc}} - Q_{\text{c,released}}| \leq \epsilon_2$

Figure 12.5 illustrates the various ways a combined cooler can meet a specific cooling load under identical environmental conditions. The optimal operating points—the Pareto front—are highlighted in the figure. The background color represents the distribution of cooling power: green indicates a greater contribution from the dry cooler, while purple indicates a greater contribution from the wet cooler. Notably, only the leftmost point relies exclusively on the dry cooler. Moving even slightly to the right results in a rapidly increasing contribution from the wet cooler.

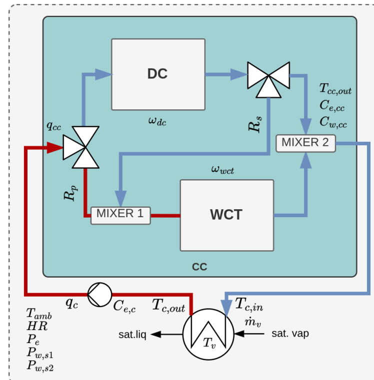

Figure 12.4: Diagram of the combined cooler

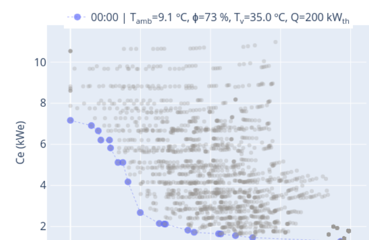

Add a background color antes del domingo

Reminder: Pareto front

When dealing with multiple objectives where no single solution is optimal, but improvements in one objective lead to trade-offs in others, a set of points is obtained that represents the best trade-offs between the objectives—known as a Pareto front[a].

[a] See Section 8.3 (Multi-objective optimization)

12.3 Horizon optimization

The problem structure is very similar to the static alternative, the main difference is that now the decision and environment vectors are composed not from the expected value for the optimization step, but an array of values from the current optimization step (i) until the end of the prediction horizon (n_{steps})[7]:

7: Bold notation is used to indicate that the variable is an array and not a single value, *e.g.* $\mathbf{x}$

Problem: CC - horizon

$$\min_{\mathbf{x}, \mathbf{e}; \theta} \quad J = f(\mathbf{x}, \mathbf{e}; \theta) = \sum_{i=1}^{n_{steps}} \left(J_{e,i} + J_{w,i}\right) \cdot T_s$$

$\forall i = 1 \dots n_{steps}$ is a notation to indicate that a condition must be held at every step i in the optimization horizon (n_{steps})

with:

$$
\begin{aligned}
&for\, i = 1 \ldots n_{steps} : \\
&\qquad J_{e,i} = C_{e,i} \cdot P_{e,i} \\
&\qquad J_{w,i} = C_{w,s1,i} \cdot P_{w,s1,i} + C_{w,s2,i} \cdot P_{w,s2,i} \\
&\qquad C_{w,s1,i} = \frac{\min(V_{avail,i}, C_{w,i} \cdot T_s)}{T_s} \\
&\qquad C_{w,s2,i} = C_{w,i} - C_{w,s1,i} \\
&\qquad V_{avail,i} = V_{avail,i-1} - C_{w,s1,i} \cdot T_s \\
&\qquad T_{cc,out,i}, C_{e,i}, C_{w,i}, T_{c,out,i} = f(q_{c,i}, R_{p,i}, R_{s,i}, \omega_{dc,i}, \omega_{wct,i}, T_{amb,i}, HR_i, T_{v,i}, \dot{m}_{v,i})
\end{aligned}
$$

- Decision variables

$$\mathbf{x} = [\mathbf{q_c}, \mathbf{R_p}, \mathbf{R_s}, \omega_{\mathrm{dc}}, \omega_{\mathrm{wct}}]$$

where $x = [x_{1,1}, \ldots\, x_{1,n_{steps}}, \ldots, x_{n_x,n_{steps}}]$

- Environment variables

$$\mathbf{e} = [\mathbf{T}_{\mathrm{amb}}, \mathbf{HR}, \mathbf{P_e}, \mathbf{P_{w,s1}}, \mathbf{P_{w,s2}}, \mathbf{V_{avail,0}}, \mathbf{T_v}, \mathbf{\dot{m}_v}]$$

where $e = [e_{1,1}, \ldots\, e_{1,n_{steps}}, \ldots, e_{n_e,n_{steps}}]$

subject to:

- Box-bounds
  - $\mathbf{w_{dc}} \in [\underline{w}_{dc}, \overline{w}_{dc}]$
  - $\mathbf{w_{wct}} \in [\underline{w}_{wct}, \overline{w}_{wct}]$
  - $\mathbf{q_c} \in [\underline{q}_c, \overline{q}_c]$
  - $\mathbf{R_p} \in [0, 1]$
  - $\mathbf{R_s} \in [0, 1]$
- Constraints, $\forall i = 1 \ldots n_{steps}$:
  - $|T_{\mathrm{cc,out},i} - T_{\mathrm{c,in},i}| \leq \epsilon_1$
  - $T_{\mathrm{c,out},i} \leq T_{v,i} - \Delta T_{\mathrm{c\text{-}v,min}}$
  - $|Q_{\mathrm{cc},i} - Q_{\mathrm{c,released},i}| \leq \epsilon_2$

This formulation allows for an arbitrary long prediction horizon, however, since forecasts for each variable in the environment are needed, it will be limited to a number of steps where reliable predictions can be obtained. On this work water availability is allocated daily so the prediction horizon is established until the end of the operation day, and it starts from the current time when the optimization is launched.

12.3.1 A discussion on solving the optimization problem

As defined, the CCS problem decision vector is composed by five variables that are direct inputs on the process[8]. But as mentioned, not any five values for these variables will yield a feasible solution, in the real system this translates to the fact that a stable operation *i.e.* steady-state would never be reached for that set of inputs. To check for feasible operation the three mentioned constraints are introduced, however, this increases the complexity of the solution space significantly, since the solution space will not be continuous, but as seen in Figure 12.6, it will be formed by islands of feasible solution space regions separated by infeasible regions. This means that finding a feasible solution is not trivial, and the optimization algorithm will need to explore the solution space-a global search algorithm-in an attempt to find the global minimum.

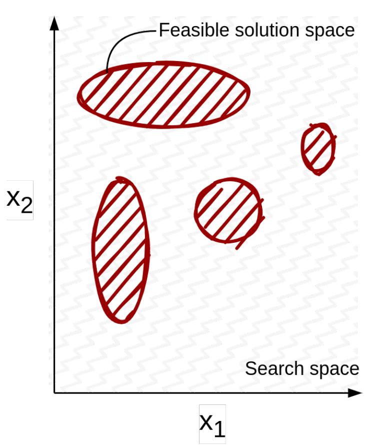

Figure 12.6: Visualization of a constrained search space for two decision variables

For one single step, most global search algorithms with multiple runs[9] were able to consistently find the global optima, this was not the case for local gradient-based algorithms, which were very sensible to the initial conditions and often converged to local minima, even when coupled with other techniques, such as Generalized Monotonic Basin Hopping [31], they struggled to consistently escape these local optima.

9: Tried algorithms include: Algoritmos probados de pygmo y Poner Gaussian también

[31]: Wales et al. (1997), "Global Optimization by Basin-Hopping and the Lowest Energy Structures of Lennard-Jones Clusters Containing up to 110 Atoms"

The problem becomes significantly more complex when the prediction horizon is extended, the decision vector grows five-fold for each additional step in the prediction horizon, and the optimization algorithm is tasked with finding a feasible solution for this much larger decision vector, in a very complex solution space, at once for all steps. The chances of finding a feasible solution decrease significantly, and this was reflected in the failure to find a single feasible solution. Even when providing an initial guess composed by the static problem solutions for each step in a 24 steps horizon, the returned solution was that same initial guess.

12.3.2 Proposed solution: Decomposition-based multi-objective optimization with trajectory planning

A two-level optimization strategy is proposed to solve a multi-step decision problem[10]. At each step of the prediction horizon, a multi-objective optimization problem is independently solved, yielding a Pareto front. A global optimization problem is then formulated to select a path through the sequence of Pareto fronts, minimizing a cumulative objective (*i.e.*, cost), akin to a pathfinding or Traveling Salesman Problem (TSP)-like over Pareto-optimal points.

10: Alternative wording: Pareto front chaining, multi-step Pareto optimization, path planning on Pareto surfaces.

The methodology is illustrated in Figure 12.7 and its components are described in the following sections.

Solving the multi-objective optimization problems

To limit the complexity of the problem, the decision space can be reduced by one by variable by analyzing how the complete model is solved and described in Section 11.4 (Complete system); firstly, the condenser can be solved just by using the recirculation flow rate (q_c), it follows the dry cooler by adding the first valve ratio (R_p) and dry cooler fan speed (ω_{dc}). The only remaining component to solve is the wet cooler. The wet cooler inlet conditions (q_{wct}, $T_{wct,in}$) can be determined by using the second valve ratio (R_s). As for the outlet conditions, from the condenser evaluation, its inlet temperature is known and it sets the value of the combined cooler outlet temperature ($T_{cc,out}$), which in turn is the result of the mixing from the DC and WCT outlet temperatures ($T_{dc,out}$ and $T_{wct,out}$, respectively).

The result of this analysis is that the wet cooler fan speed is not a decision variable anymore, but an output of the model, which can be computed by inverting the wet cooler model, where an outlet temperature is provided as input, and the fan speed is computed as an output. Summarizing, the decision vector can be reduced from five to four variables:[11]

11: This reasoning works only for a system with this particular configuration, a different combined cooler layout would require a different analysis.

$$x = [q_c, R_p, R_s, \omega_{dc}]$$

More importantly, now the optimization algorithm does not need to find a set of five inputs that produce a feasible solution in a complex solution space, but only four values from which a feasible wet cooling tower fan speed exists[12], thus greatly simplifying the problem.

12: *i. e.* within its bounds $\omega_{wct} \in [\underline{\omega}_{wct}, \overline{\omega}_{wct}]$

0. Decompose the problem horizon into its n steps elements.

1. Solve a multi-objective optimization problem, independently for each step, to obtain a set of pareto fronts:

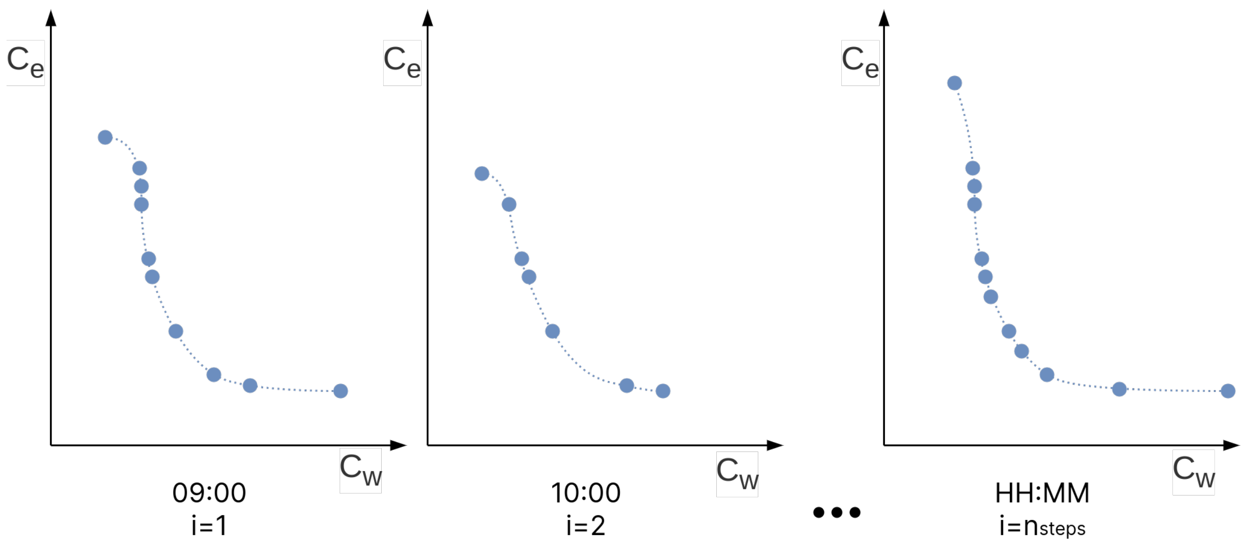

2. Select a path through these pareto fronts that minimizes a global objective: the cumulative operation cost of operation

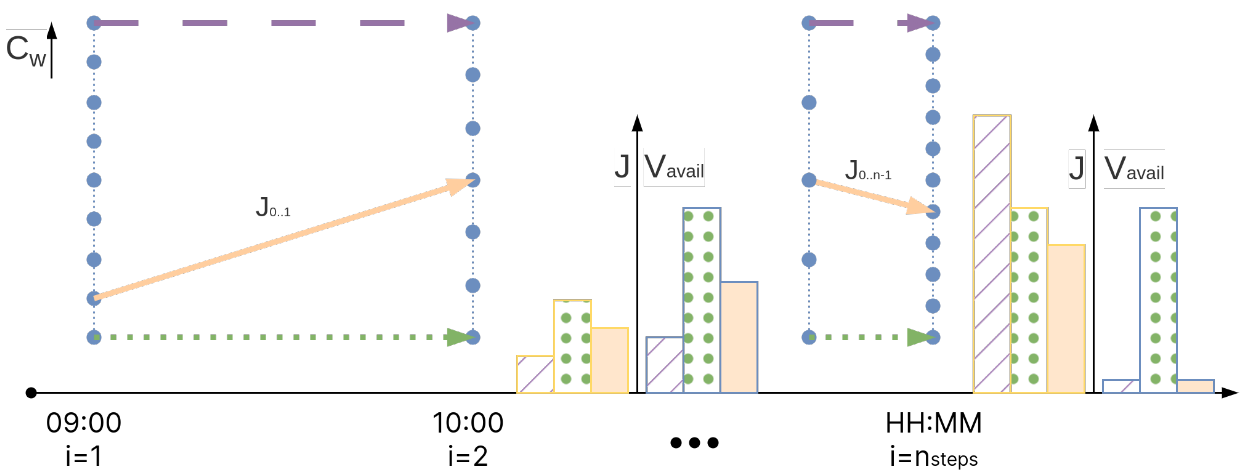

Figure 12.7: Proposed methodology. Decomposition-based multi-objective optimization with trajectory planning. In step 2. three paths are illustrated: a water-greedy dash-purple (- -) path, a water-conservative green-dotted path (. .) and a compromise-approach solid-*orangey* path (—)

A straightforward approach to solve the multi-objective optimization is to do a grid-search over the decision space, evaluating the model for every combination of decision variables, and then storing only the points for which a feasible ω_{wct} exists. This approach is not recommended for large decision spaces, but for the four-dimensional decision space and with a model that can be evaluated in fractions of a second, it is feasible.

Next, the Pareto front is computed from the feasible points, which are evaluated in terms of the two consumptions: electricity (C_e) and water (C_w). By definition, the Pareto front is the set of points that cannot be improved in one objective without worsening the other, and it is computed by checking for each point if there is another point that is better in both objectives, and if so, it is removed from the set of feasible points. The remaining points form the Pareto front. This process is repeated for each step in the prediction horizon, resulting in a set of Pareto fronts, one for each step, as visualized in Figure 12.7–**1**.

Path selection subproblem

The path selection subproblem is a combinatorial optimization problem over a layered weighted directed graph, where each layer corresponds to a time step in the prediction horizon, and each node in a layer represents a point on the corresponding Pareto front. The objective is to find a path $\mathbf{p} = (p_1, p_2, \ldots, p_{n_{\text{steps}}})$, where p_i is the selected node at time step i, that minimizes the total cumulative cost along the path (J). The problem can be formulated as:

$$\min_{\mathbf{p}} \quad J = \sum_{i=1}^{n_{\text{steps}}-1} C_{\text{transition}}(p_i, p_{i+1})$$

Each transition cost $C_{\text{transition}}(p_i, p_{i+1})$ depends on both consumptions (*i.e.* electricity and water consumption) of the nodes p_i and p_{i+1}, as well as a dynamic price function that depends on the path history. Specifically, the transition cost is correlated to the current resource availability ($V_{avail,i}$)[13] and will depend on the current state of the system, which is a function of the previous decisions. This is a very simple calculation that can be computed almost instantly, and it is the only information needed to compute the transition costs between two points in the Pareto front:

13: See Equations (12.1)–(12.3)

$$C_{\text{transition}}(p_i, p_{i+1}) = P_e(i) \cdot C_e(p_{i+1}) + P_w(i) \cdot C_w(p_{i+1})$$

where:

- $C_e(p_{i+1})$, $C_w(p_{i+1})$: electricity and water consumption at node p_{i+1}
- $P_e(i)$, $P_w(i)$: price coefficients for electricity and water at step i, which may be dependent on the previously selected nodes (*i.e.*, the path so far)

Prices $P_e(i)$, $P_w(i)$ depend on prior path decisions, this introduces path-dependency into the cost function, and makes the problem non-trivial to solve via simple shortest path algorithms. The problem could be handled via dynamic programming, graph search (like Dijkstra or A*), or metaheuristics such as genetic algorithms.

The subproblem is illustrated in Figure 12.7–2. Each node represents a point in the Pareto front of a step, and edges represent the transition costs between these points, that is, the cumulative cost so far ($J_{0..i}$). Three paths are illustrated in Figure 12.7–2. The dash-purple (- -) path is a path that chooses nodes with a high water use[14], so in the first split it can be seen it achieves the lowest cost of operation, but also leaves the least water available for the next steps, resulting in a higher total cost of operation. On the other hand, the green-dotted path (..) chooses the nodes with the lowest water use, this translates in a consistently higher cost of operation and leaving some water available at the end of the horizon. Because of the formulation of the problem, this is sub-optimal since this unused water is considered lost. Finally, the solid-*orangey* path (–) is a compromise between the two, it uses water more efficiently, leaving no water available at the end of the horizon and minimizing the overall cost of operation.

14: In Figure 12.7, nodes are ordered with increasing values of C_w from bottom to top.

Combined cooling pilot plant at Plataforma Solar de Almería 13

TL;DR

In this chapter a detailed description of the combined cooling pilot plant at PSA is provided including a Piping and Instrumentation Diagram (P&ID) diagram and the methodology followed to perform the experimentation and data-processing. Three experimental campaigns for the WCT with XX, XX and XX different operating points and one for the DC with XX operating points are processed and made openly available in public repositories.

Introduction

The combined cooling pilot plant at Plataforma Solar de Almería is a unique facility that integrates a wet cooling tower and a dry cooler in a flexible hydraulic configuration. It allows for the study and validation of different cooling strategies and the development of models.

completar esta sección antes del domingo

...

This chapter describes the plant in Section 13.1 (Plant description) and the experimental campaigns carried out in Section 13.2 (Experimental campaigns).

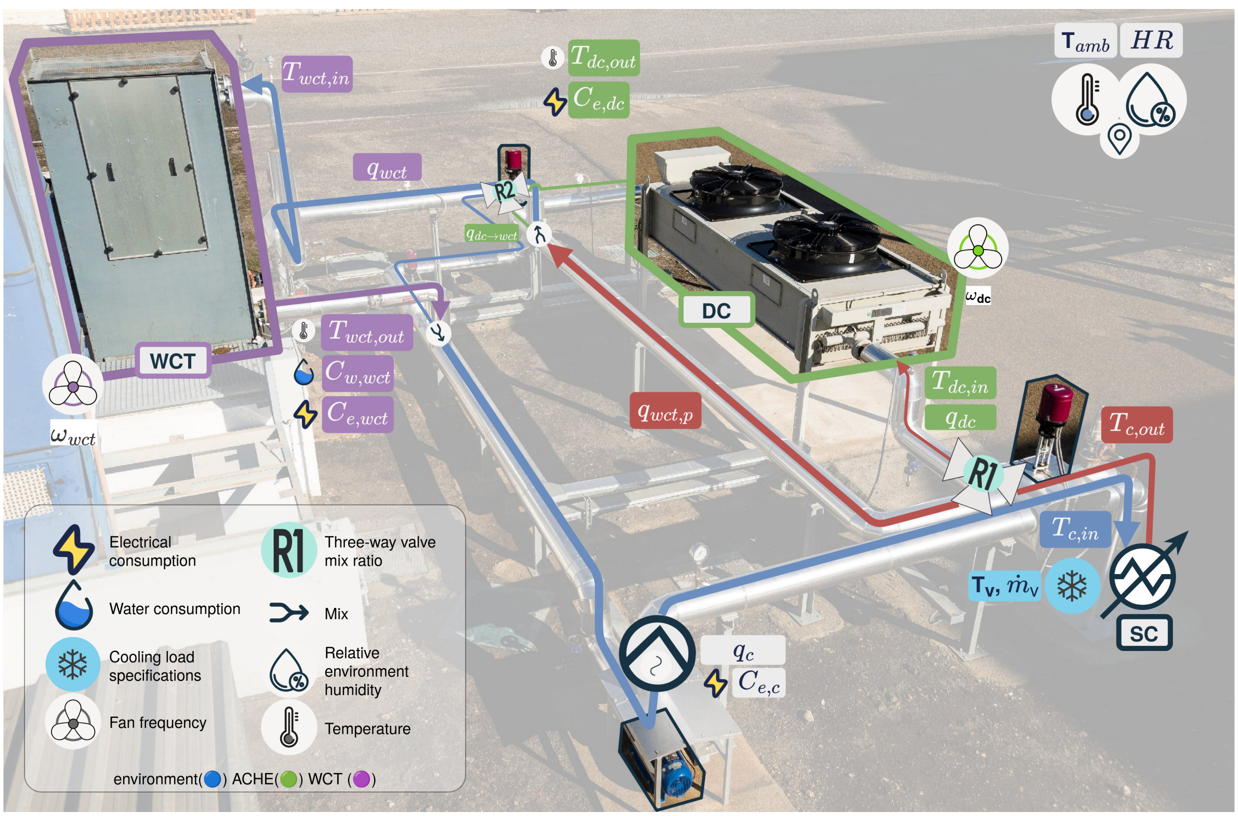

Figure 13.1: PSA combined cooling system facility

13.1 Plant description

Figure 13.2: Back view of the WCT.

The pilot plant of combined cooling systems located at PSA (see the layout in Figure 13.3) consists of three circuits: cooling, exchange and heating. In the cooling circuit (see a picture in Figure 13.2), water circulating inside the tube bundle of a Surface Condenser (SC) can be cooled through a Wet Cooling Tower and/or a Dry Cooling Tower (type Air Cooled Heat Exchanger, ACHE), both with a designed thermal power of 204 kW$_{th}$. In the exchange circuit, a saturated steam generator of 80 kW$_{th}$ (on the design point), generates steam at different pressures (in the range between 82 mbar and 200 mbar), which is in turn condensed in the surface condenser. In this way, the steam transfers its latent heat of condensation to the refrigeration water, that is heated. Finally, in the heating circuit, a solar field with a thermal power of 300 kW$_{th}$ at the design point, provides the energy required by the steam generator, in the form of hot water. It is a unique, very flexible, fully instrumented and versatile facility, able to operate in different operation modes: series and parallel mode, conventional dry-only mode (all water flow is cooled through the dry cooling tower) and wet-only mode (all water flow is cooled through the wet cooling tower). The instrumentation related to the WCT is described in Table Table 13.1. Note that the sensors measuring the air velocity and temperature and relative humidity at the outlet area of the wet cooling tower have not been installed in the plant. Portable sensors were used instead in some experiments, as described in Section ??.

In regards to operational aspects of the system, note that the cooling water and air flow rates at the experimental facility ($\dot{m}_w$, and air, $\dot{m}_a$, respectively), are modified with the *Pump 1* and the fan frequency percentage `SC-001`, respectively (see Figure 13.3).

Table 13.1: Characteristics of instrumentation ([a] value of the temperature in °C, [b] of reading, [c] full scale, [d] mean value).

Measured variable	Instrument	Range	Measurement uncertainty
Water temperature (`TT-001`, `TT-006`)	Pt100	0 - 100 °C	0.03 + 0.005·T^a
Cooling water flow rate (`FT-001`)	Vortex flow meter	9.8 - 25 m^3/h	± 0.65 % o.r.[b]
Water flow rate (`FT-004`)	Paddle wheel flow meter	0.05 - 2 m^3/h	± 0.5 % of F.S[c] + 2.5 % o.r
Ambient temperature	Pt1000	-40 - 60 °C	± 0.4 @20 °C
Relative humidity	Capacitive sensor	0 - 98%	± 3 % o.r @20 °C
Air velocity	Impeller anemometer	0.1-15 m s^{-1}	± 0.1 m s^{-1} + 1.5 % o.r
Outlet air temperature	Pt100	-20-70°C	±0.5°C
Outlet air humidity	Capacitive sensor	0-100%	± 2%

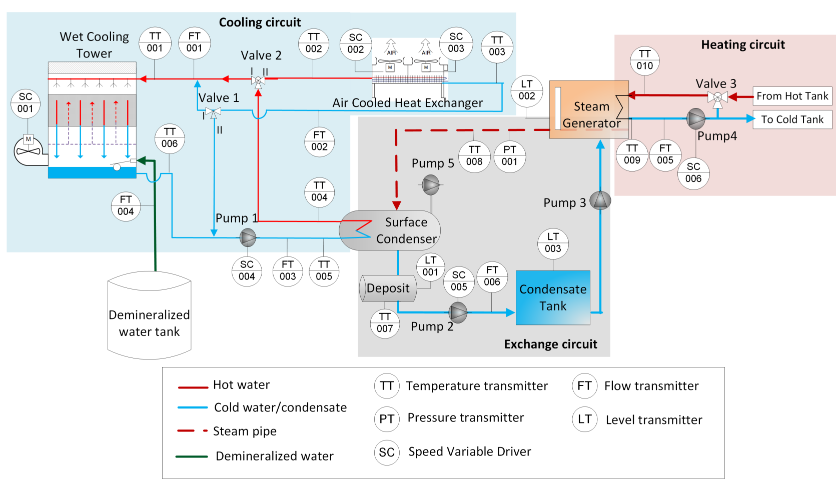

Figure 13.3: Layout of combined cooling systems pilot plant at PSA.

13.2 Experimental campaigns

With the aim of characterizing and developing models for this novel facility, over the years several experimental campaigns have been carried out. In particular, three different experimental campaigns have been performed to characterize the WCT specifically, while a campaign was also carried out to characterize the DC.

13.3 Experimental campaigns for the wet cooling tower

A total of 132 steady-state experimental points have been obtained. These data cover a large variety of ambient conditions (different seasons, days and nights) and thermal loads (from 27 kW to 207 kW). The objective of the experimental campaigns is to develop and validate two modelling strategies for the performance evaluation of the WCT[1].

1: See Section 11.1 (Wet cooler)

The normative framework followed to carry out the experiments, in order to ensure stable conditions, has been the standards `UNE 13741` [32] and the Spanish CTI [33]. These standards specify the test duration and the allowed variations of the most representative ambient and operating magnitudes (water flow rate, heat load, cooling tower range, wet-bulb and dry-bulb temperatures and wind velocity) during the tests. Although the duration of the test should not be less than one hour according to the standards, due to the low capacity of the WCT in the PSA pilot plant and the operational experience, the duration of the tests has been reduced to up to 30 minutes. Once stable conditions are maintained during the defined interval time, the average and deviations values of each measurement are calculated in order to check that they are within the allowable limits of the norm, which finally lead to a valid steady-state operating point.

[32]: UNE (2004), *Thermal Performance Acceptance Testing of Mechanical Draught Series Wet Cooling Towers*

[33]: CTI (2000), *Code Tower, Standard Specifications. Acceptance Test Code for Water Cooling Towers*

Figure 13.4 shows the main variables involved in one of the experiments performed at the pilot plant at constant air flow rate (f_{fan}=25 %). As can be observed, there are two time intervals in this case, in which the process is at stationary conditions according to the normative framework mentioned. In order to process the results of the experimental tests and identify valid time intervals, such as the ones shown in this example, a function has been implemented in the *MATLAB* environment. This function identifies whether the standard criteria is met and calculates the mean values of the required variables.

The data from the different experimental campaigns is available at [**palenzuela_steadystate_2024a**, 34].

palenzuela_steadystate_2024a, [34]: Serrano et al. (2024), "Wet Cooling Tower Performance Prediction in CSP Plants"

13.3.1 Experimental campaign 1 – Exp 1

This campaign was specifically designed for the calibration of the physical model. In total, 19 experimental tests were performed at the combined cooling pilot plant at PSA. The physical model focuses on the calculation of the Merkel number which, according to the literature ASHRAE [28], is not a constant value. Instead, it varies depending on the operating conditions (water-to-air mass flow ratio, $\dot{m}_w/\dot{m}_a$). Therefore, the experimental campaign has been designed to cover different water-to-air mass flow ratios. Both variables, the water and the air flow rates, were varied within the allowable range for plant operation. In the case of the water flow rate, it ranged from 8 m^3/h to 22 m^3/h, and in the case of the air mass flow rate, it was modified by changing the fan frequency from 12.5 Hz to 50 Hz (fan frequency percentage, f_{fan}, from 25 % to 100 %). The magnitudes required to experimentally determine the air mass flow rate (air velocity and air temperature and relative humidity) were measured at the outlet area of the

[28]: Ashrae (2004), "HVAC Systems and Equipment"

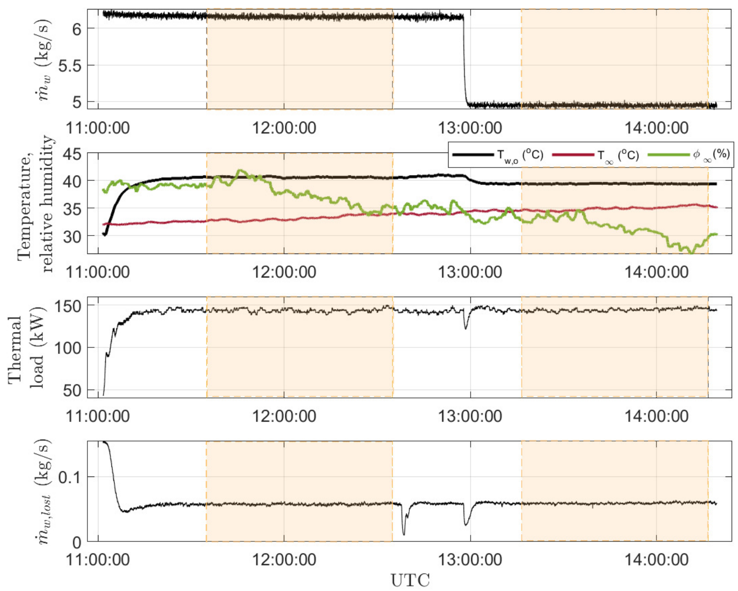

Figure 13.4: Example of one experiment at the pilot plant in July with two valid steady-state operating points.

2: Using the sensors listed in Table 13.1

cooling tower[2]. The outlet area was divided into 9 quadrants and the above mentioned magnitudes were registered at the center of each quadrant. The obtained values were averaged to determine the mean velocity, temperature and relative humidity used in the air mass flow rate calculation.

3: This enables to obtain the air mass flow rate at the outlet of the cooling tower, $\dot{m}_a$, using the permanent sensors installed in the facility

Following the same experimental procedure, air velocity, temperature and humidity maps were measured for 8 different f_{fan} levels (ranging from 30 % to 100 % in 10 % intervals)[3].

The range of air and water mass flow rates are 1.16-4.32 kg/s and 2.17-6.15 kg/s, respectively. Regarding the environmental conditions, these were quite similar for all tests in the campaign: high ambient temperatures (ranging between 32 °C and 41 °C), and low ambient relative humidities (between 13 % and 40 %) since the experiments were carried out during the summer season.

13.3.2 Experimental campaign 2 – Exp 2

The data required for data-driven models depends on several factors such as the complexity of the model and the error allowed or the diversity of the inputs. With the aim of obtaining a reliable model for the WCT, data collected over several years of operation of the combined cooling system have been used for tuning. They are a set of 115 stationary data covering the following operating ranges: ambient temperature, T_∞, [9-39] °C, ambient humidity, ϕ_∞, [10-87] %, inlet water temperature, $T_{w,i}$ [33-41] °C, cooling water flow rate, q_w, [6-23] m^3/h and fan frequency percentage, f_{fan} [21-94] %. The thermal load in these tests varies in the range of [27-178] kW_{th}. The number of steady-state data obtained is a reasonable value when compared to other similar data-driven models of counter-flow cooling towers, as in the case of [24], where 81 experimental points were collected for training and testing.[4]

4: Reminder, dataset is available at [palenzuela_steadystate_2024a]

13.3.3 Experimental campaign 3 – Exp 3

With the aim of validating and comparing different modelling approaches, a dataset of 17 tests (different from the ones taken for experimental campaigns 1 and 2) has been compiled. This experimental campaign was designed using a design of experiments based on full factorial design with 4 factors and 2 levels (low and high), whose values are shown in Table 13.2.

An additional test at design operating conditions of the WCT ($T_{b,\infty}$=21 °C, $T_{w,i}$=40 °C, $\dot{m}_w$=6.9 kg/s and $T_{w,i} - T_{w,o}$=7 °C) has been also included in this test campaign, where $T_{b,\infty}$ is the ambient wet bulb temperature and $T_{w,o}$ the temperature of the water at the outlet of the WCT.

Table 13.2: Design of experiments for model comparison.

Variable	Low level	High level
T_b (°C)	≤ 10	≥ 15
$T_{w,i}$ (°C)	≤ 37	≥ 39
$\dot{m}_w$ (kg/s)	≤ 3.3	≥ 5
$T_{w,i} - T_{w,o}$ (°C)	≤ 7	≥ 8

13.3.4 Experimental campaigns for the dry cooler

14 Validation in the combined cooling pilot plant

To Do

After the chapter is complete, find and replace all mentions to RBF, ANN, RMSE and all other acronyms with the acronym with `\gls`.

14.1 Modelling

The two main components of the system (WCT and DC) are modelled with different approaches and compared in detail. Afterward, the integration of the selected modelling approach with the rest of the system components (Section 11.3) is validated in Section 14.1.5 (Complete system model validation).

14.1.1 Wet cooler model alternatives comparison and validation

Physical model

As previously mentioned[1], three experimental campaigns have been performed, shown in Figure 14.1 as Exp 1, Exp 2, and Exp 3. Exp 1 corresponds to the Poppe model calibration campaign and it was designed for the calibration of the first principles model. The aims of such campaign was to fit a function (mapping) that relates the air mass flow rate at the outlet of the tower, $\dot{m}_a$, with the frequency of the fan, f_{fan}:

1: See Section 13.3 (Experimental campaigns for the wet cooling tower)

Lidia, aquí la correlación no usa la temperatura ambiente

$$\dot{m}_a = -0.0014 f_{fan}^2 + 0.1743 f_{fan} - 0.7251. \tag{14.1}$$

and to calibrate a WCT performance coefficient: the Merkel number, Me. Figure 14.2 shows the variation of the Merkel number as a function of the water-to-air mass flow ratio ($\dot{m}_w/\dot{m}_a$) using data from Exp1. As can be seen, the Me decreases with $\dot{m}_w/\dot{m}_a$ values following a linear trend on log-log scale.

Make text in figure larger

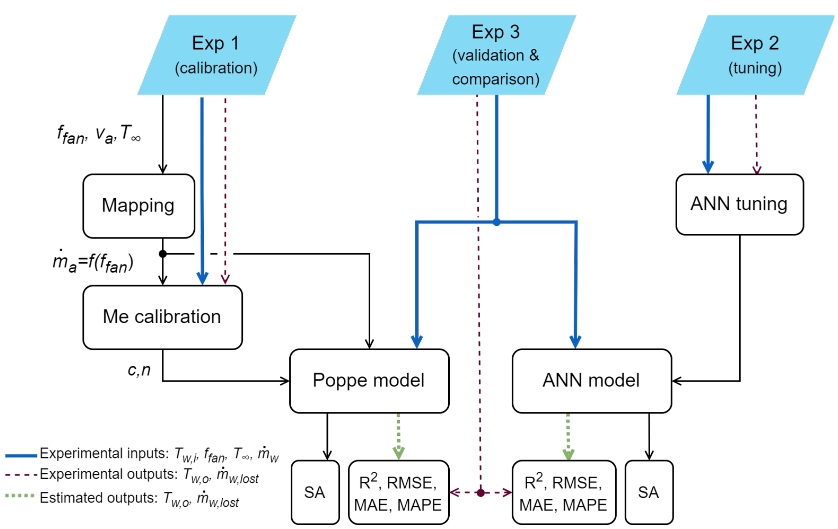

Figure 14.1: Calibration, tuning, validation and comparison procedure

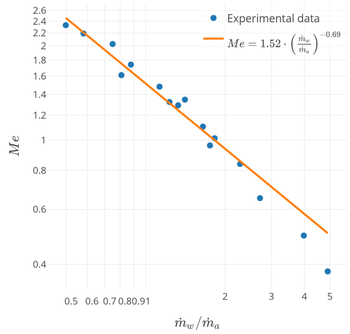

Figure 14.2: Experimental results for the Me number as a function of $\dot{m}_w/\dot{m}_a$.

Following the correlation for the Merkel number of a wet cooling tower described in Section 11.1.1, the parameters c and n obtained from the data fitting are 1.516 and 0.693, respectively.

Data-driven

In order to generate the data-driven from first-principles alternative, the most relevant input variables identified in Section **??** are discretized using a fixed number of resolution steps for each variable, within ranges based on expected operating conditions, as defined in Table 14.1.

Table 14.1: Bounds and discretization of the model input variables.

x	Units	lb	ub	n
T_{amb}	°C	3	50	7
ΔT_{amb-in}	°C	3	30	7
q_{dc}	m^3/h	0.00	1.00	5
ω_{dc}	%	11.00	99.18	10
ω_{wct}	%	21.00	93.42	10

Figure 14.3 shows the generated input space distribution. The upper plot shows the frequency distribution of the samples while the lower one the actual values per input, where the x-axis represents the samples and the y-axis the values for each of the input variables.

Prediction capabilities

Tabla tocha añadiendo casos (GPR, DD from FP, RF, GB)

The results of each modelling alternative and its comparison can be visualized in Figure 14.4 and Table 14.4. The results of each modelling alternative and its comparison can be visualized Figure 14.4 shows the results obtained with the models using Exp 3. It shows the perfect fit together with the results obtained with Poppe's model, MIMO FF, cascade CF, and MIMO RBF. In Table 14.4, the performance of the studied modelling approaches are included for the different performance metrics[2]. T represents the performance metric value for the training / calibration dataset (Exp 1 or Exp 2 depending on the case), and V for the validation and comparison one (Exp 3). In all cases the model representing each alternative is in the best case scenario, *i. e.* maximum number of points available. On the other hand, `s.u.` indicates that the units of the column are the same as from the source variable.

2: Described in Section 5.1

Comparing both modelling approaches (see Figure 14.4), it can be outlined that both models provide a good prediction of the output variables, falling most of the discrepancies (errors) within the uncertainty range. Poppe's model provides a better prediction of the outlet temperature, obtaining an RMSE of 0.33 °C and an R^2 of 0.98. In comparison, the best ANN alternative (RBF MIMO) has a slight worse performance with an RMSE of 0.51 °C and $R^2 = 0.95$. In terms of water consumption, the physical model has a better prediction accuracy in terms of RMSE and R^2 (8.5 l/h and 0.97) compared to 11.24 l/h and 0.95 for the best ANN model (cascade CF). It can be stated that, although the results are better for the physical model (specially in the case of the outlet temperature prediction), both approaches produce valid results with high accuracy levels.

Experimental data requirements

In order to estimate the minimum number of tests required to obtain satisfactory results with both modelling strategies, an analysis was performed in which each modelling alternative was calibrated/tuned for different case studies with different amounts of available data, and then the performance metrics were evaluated. In this way, trends in the predictive accuracy of the models as a function of the available data can be identified. When the variation becomes small, it can be stated that the model has converged and adding more information provides diminishing returns.

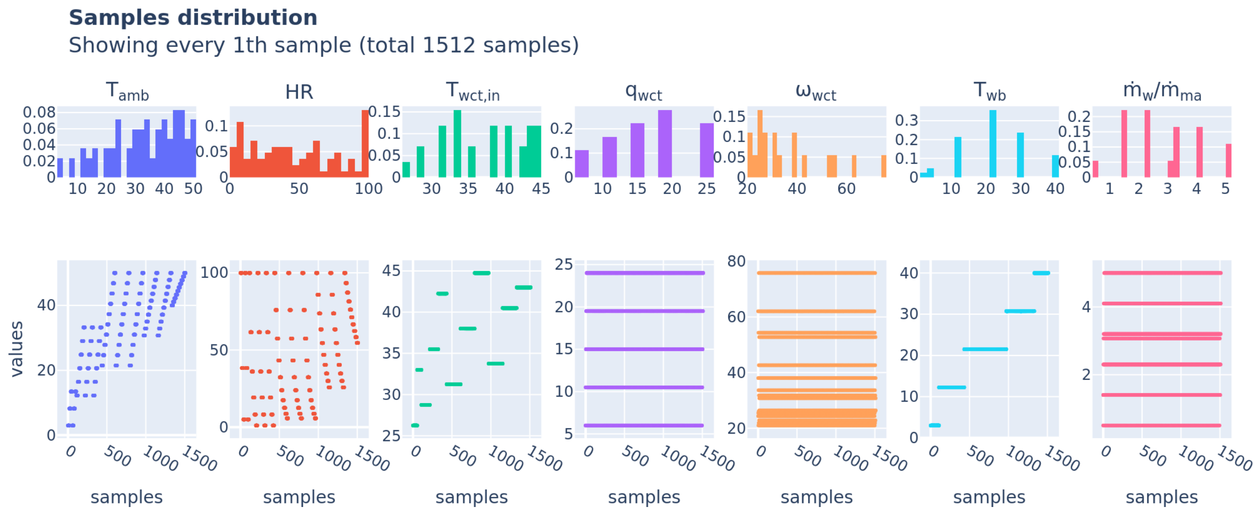

Figure 14.3: Data-driven from first-principles. Samples distribution visualization.

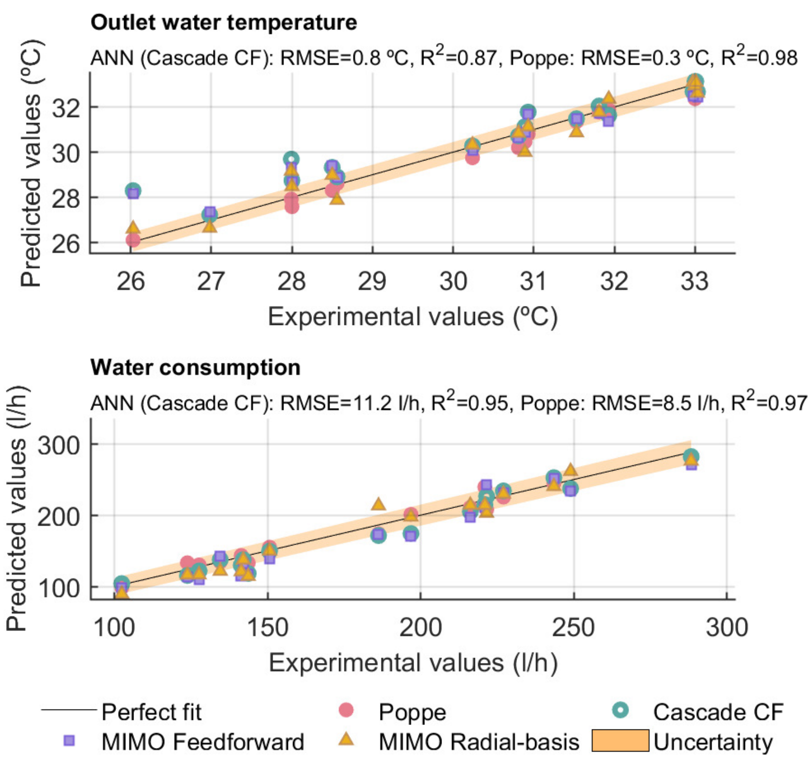

Figure 14.4: Model results obtained with Poppe and ANN models and data of Exp3

Table 14.2: Summary table of the prediction results obtained with the different modelling approaches studied.

Predicted variable	Modelling alternative	Model config	Topology	Performance metric R^2 (-)		RMSE (s.u.)		MAE (s.u.)		MAPE (%)		Evaluation time (s)
				T	V	T	V	T	V	T	V	
$T_{o,w}$ (°C)	Poppe	-	-	-	0.98	-	0.33	-	0.27	-	0.87	6.288
	Feedforward ANN	MIMO	20-2	0.93	0.89	0.52	0.74	0.37	0.51	1.22	1.78	0.004
	Cascade-forward ANN	MIMO	10-5-2	0.93	0.90	0.50	0.70	0.35	0.47	1.15	1.65	0.004
	Radial basis ANN	MIMO	37-2	0.99	0.95	0.23	0.51	0.18	0.40	0.57	1.35	0.004
	Feedforward ANN	Cascade	10-10-1	0.94	0.89	0.46	0.72	0.32	0.49	1.05	1.71	0.007
	Cascade-forward ANN	Cascade	10-10-1	0.94	0.87	0.46	0.79	0.31	0.52	1.02	1.82	0.008
	Radial basis ANN	Cascade	92-1	0.99	0.69	0.23	1.22	0.08	0.92	0.25	3.20	0.008
$\dot{m}_{w,lost}$ (l/h)	Poppe	-	-	-	0.97	-	8.47	-	6.74	-	3.74	6.288
	Feedforward ANN	MIMO	20-2	0.95	0.90	11.75	16.27	9.47	14.53	7.74	8.44	0.004
	Cascade-forward ANN	MIMO	10-5-2	0.96	0.94	10.52	12.68	8.23	10.96	6.68	6.33	0.004
	Radial basis ANN	MIMO	37-2	0.99	0.93	4.88	13.86	3.67	10.93	2.94	6.76	0.004
	Feedforward ANN	Cascade	20-1	0.97	0.93	9.64	13.57	7.50	11.18	6.12	6.39	0.007
	Cascade-forward ANN	Cascade	10-10-1	0.97	0.95	8.52	11.24	6.18	9.15	4.92	5.21	0.008
	Radial basis ANN	Cascade	29-1	0.98	0.91	7.63	15.70	4.54	12.41	4.13	6.93	0.008

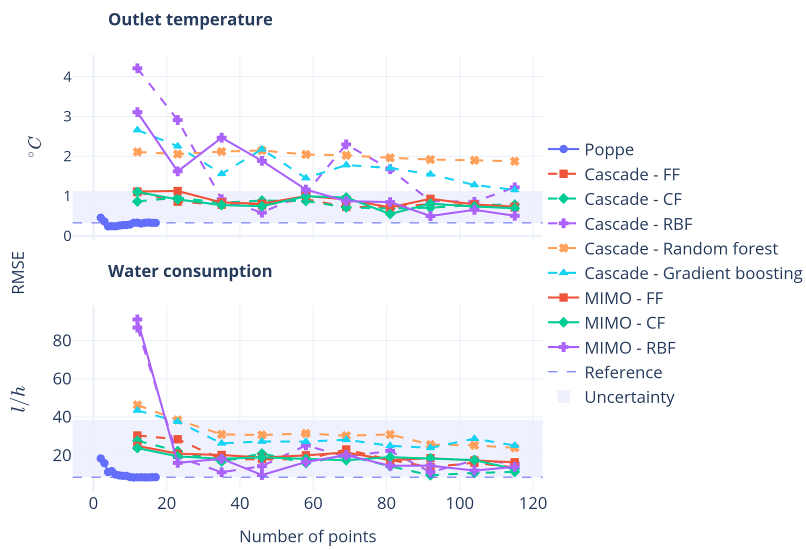

Figure 14.5: RMSE evolution as a function of the number of points used for calibration/-training of the Poppe's and data-driven approaches

For the physical model, the number of tests from Exp 1, used to calibrate Me correlation, was varied from 2 up to 16 data points added sequentially. In the case of the ANN models, the available tuning data (Exp 2) was increased in steps of 10 %, starting from the availability of 10 % up to the entire data set (100 %).

In both cases, the criteria for selecting the data was not random, but it was done by applying physical knowledge. The water-to-air mass flow ratio, $\dot{m}_w/\dot{m}_a$, is a good indicator for selecting the operation points to be fed to the model. The trend observed in Figure 14.2 (decreasing Me for increasing $\dot{m}_w/\dot{m}_a$) has been extensively reported in the literature. This behavior is explained by the increase in the amount of water per unit of air that lead to a less effective cooling [35]. The situation corresponding to the minimum $\dot{m}_w/\dot{m}_a$ can be interpreted as the maximum air flow rate for a given water flow rate to be cooled. This results in the maximum driving force and, therefore, maximum Merkel number. As $\dot{m}_a$ decreases progressively, the driving force decreases for a given $\dot{m}_w$, and Me decreases accordingly. Based on this knowledge, the selection starts by choosing extreme points for the water-to-air mass flow ratio in the Me-$\dot{m}_a/\dot{m}_w$ relationship from the available data, which gives information of the system operating in its limits. Subsequently intermediate points are added, covering this way the whole operating range of the cooling system.

[35]: Ruiz et al. (2022), "Thermal Performance and Emissions Analysis of a New Cooling Tower Prototype"

The results of this study are presented in Figure 14.5, where the x-axis represents the number of available data points and the y-axis a model performance metric (RMSE) obtained when the model outputs are compared to data from Exp 3. From the results obtained, it can be clearly seen the advantage of the physical model in terms of data requirements, since with the minimal amount of points, good results are obtained, and by enlarging the available data points to 8-10, low variation in the RMSE evolution can be observed for both predicted variables. In the case of the ANN-based approaches, the results differ depending on the ANN alternative.

In terms of the outlet temperature, very good results (low error and variation) are obtained with the minimal dataset (10 % of available data, 12 data points) for feedforward and cascade-forward in any configuration (MIMO and cascade). If more data is added, RMSE is reduced from 1.1 up to 0.7 °C. Although the MIMO RBF outperforms the results of the other ANN alternatives, it does so only from 90 points onwards. For this case, the downward trend is much more noticeable but constant, which can not be stated for the cascade RBF, displaying an erratic evolution up to 70 points.

Similar conclusions can be drawn for the water consumption, except that in this case the two RBF configurations achieve satisfactory results much earlier, starting from 23 points.

Summarizing, both modelling approaches, Poppe's model and ANNs, produce satisfactory results since their predictions fall well within the range of uncertainty for all the case studies, although the obtained results, in terms of RMSE, favor the physical model. Therefore, while the ANN model benefits from as much data as possible, the Poppe model is already able to produce satisfactory results with just two properly selected points. These two points are easy to identify in advance because they are related to the maximum and minimum $\dot{m}_w/\dot{m}_a$ ratio of the wet cooling tower. In practice, to minimize the error prediction, around 5 points are often used. Out of the ANN alternatives, considering both output variables, if less than 70 data points are available, cascade-forward and feedforward alternatives with any configuration are the best option, producing satisfactory results with as low as 10 points. On the other hand, if enough data is available, MIMO RBF should be considered as a strong candidate, but not in the cascade configuration alternative.

Sensitivity analysis

In Figure 14.6, only total-order sensitivity indices are represented in the y-axis for the two output variables (outlet temperature on the top and water consumption on the bottom). Its value ranges from 0 to 1, where 0 means the variable has no effect, and 1 means it has a significant effect on the output[3]. The x-axis represents the system's inputs and includes a bar for some of the obtained models with different calibration or training data points.

Comparing the results obtained for the different modelling approaches in Figure 14.6, it can be seen that very homogeneous results are obtained in all cases, except for the Cascade RBF case, which was the worst performing of all the alternatives. These results serve to confirm that, at least from a sensitivity analysis point of view, all valid approaches are similarly sensitive to variations in the same inputs, which is desirable since they are trying to predict the same physical system. In the case of Cascade RBF, a discrepancy can be observed; less relevant input variables (T_{amb} and ϕ_∞) are overestimated and overall higher uncertainties in sensitivity are observed.

It is also important to highlight that the observed results are in agreement with the underlying physics of the heat and mass transfer processes occurring in the exchange area of the tower. The frequency of the fan and the volumetric flow

Reminder: How to interpret Sensitivity Analysis (SA) results

The results are different sensitivity indices such as total sensitivity indices (total-order), first-order sensitivity indices (first-order), and interaction sensitivity indices (second-order). First-order measures the direct effect of an input variable on the output, excluding interaction effects with other variables, while the second-order measures specifically these interaction effects. Finally, total-order indices account for the total effect of an input variable, including both direct and interaction effects.[a]

[a] More in Chapter 6 (Sensitivity analysis).

3: values can go slightly above 1 due to computing errors. This is due to the Sobol' sequence sample generator producing some unfeasible test samples that need to be discarded

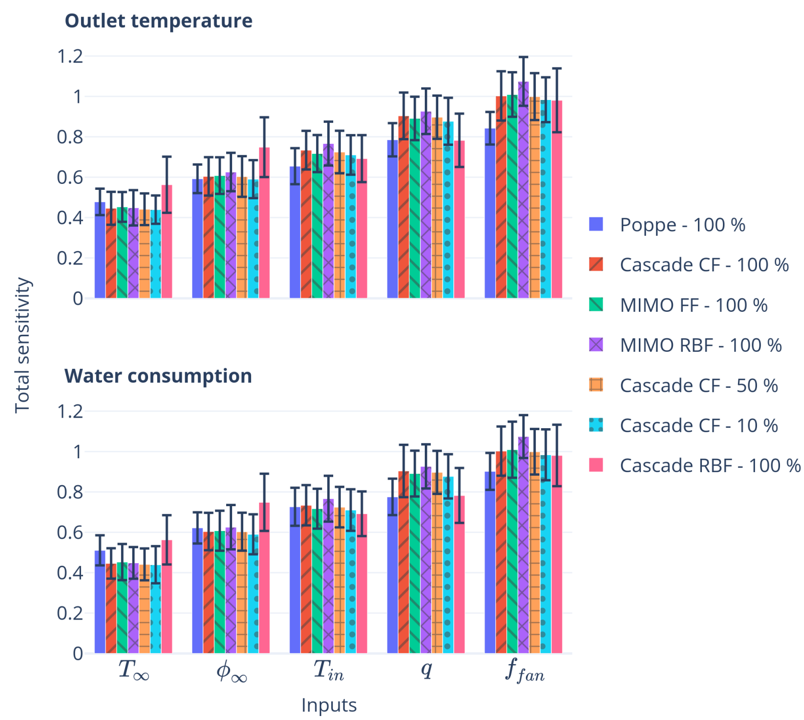

Figure 14.6: Sobol's sensitivity analysis result for different case studies

rate are directly related to $\dot{m}_a$ and $\dot{m}_w$, respectively, and they have a high influence on the heat transfer coefficients. These coefficients govern the evaporation processes, which impact the evaporation rate (water lost due evaporation) and the outlet water temperature. On the other hand, the ambient conditions and the inlet water temperature also affect the outputs, but less significantly, since the driving force for the evaporation is the difference between the inlet air enthalpy and the enthalpy of saturated air evaluated at water temperature.

14.1.2 Dry cooler model alternatives comparison and validation

Physical model

Data-driven

In order to generate the data-driven from first-principles alternative, the most relevant input variables identified in Section 11.2.2 are discretized using a fixed number of resolution steps for each variable, within ranges based on expected operating conditions, as defined in Table 14.3. and Section **??** (**??**) visualizes the generated input space distribution where it can be appreciated that the samples are well distributed across the entire input space.

Table 14.3: Bounds and discretization of the model input variables.

$\mathbf{x}$	Units	lb	ub	n
T_{amb}	°C	3	50	7
$\Delta T_{amb-dc,in}$	°C	3	30	7
q_{dc}	m^3/h	6	24	7
$T_{dc,in}$	°C	25	45	-
ω_{dc}	%	11	99.18	6

Prediction capabilities

Tabla tocha añadiendo casos (GPR, DD from FP, RF, GB)

completar esta sección antes

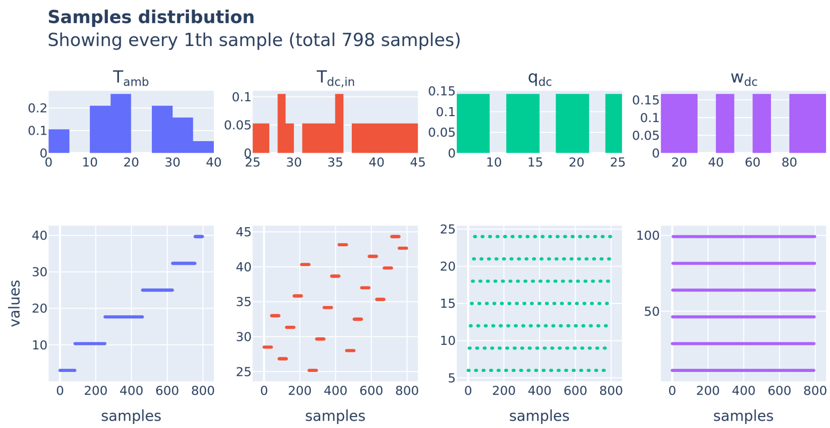

Figure 14.7: Data-driven from first-principles. Samples distribution visualization.

Table 14.4: Summary table of the prediction results obtained with the different modelling approaches studied.

Predicted variable	Modelling alternative	Model config	Topology	Performance metric R^2 (-)		RMSE (s.u.)		MAE (s.u.)		MAPE (%)		Evaluation time (s)
				T	V	T	V	T	V	T	V	
$T_{o,w}$ (°C)	Poppe	-	-	-	0.98	-	0.33	-	0.27	-	0.87	6.288
	Feedforward ANN	MIMO	20-2	0.93	0.89	0.52	0.74	0.37	0.51	1.22	1.78	0.004
	Cascade-forward ANN	MIMO	10-5-2	0.93	0.90	0.50	0.70	0.35	0.47	1.15	1.65	0.004
	Radial basis ANN	MIMO	37-2	0.99	0.95	0.23	0.51	0.18	0.40	0.57	1.35	0.004
	Feedforward ANN	Cascade	10-10-1	0.94	0.89	0.46	0.72	0.32	0.49	1.05	1.71	0.007
	Cascade-forward ANN	Cascade	10-10-1	0.94	0.87	0.46	0.79	0.31	0.52	1.02	1.82	0.008
	Radial basis ANN	Cascade	92-1	0.99	0.69	0.23	1.22	0.08	0.92	0.25	3.20	0.008

Experimental data requirements

Sensitivity analysis

14.1.3 Main components modelling conclusions

This section presents a comparison between two modelling alternatives: data-driven and first-principles. It applies to wet cooling towers and dry coolers, specifically to ACHE. The main conclusions obtained during the investigation and final recommendations can be summarized as follows:

Wet cooling tower

Regarding the prediction of the output variables, in the case of the outlet water temperature, both models reported good results, with low errors falling within the uncertainty range of the experimental equipment. Nonetheless, the physical model performs better than the best data-driven alternative (MIMO RBF): $R^2 = 0.98$ and RMSE= 0.33 °C compared to $R^2 = 0.95$ and RMSE= 0.51 °C, respectively.

Pendiente de actualizar estas conclusiones con resultados actualizados

For the predictions of water consumption, it was shown that the Poppe model accurately predicts this variable, with results of $R^2 = 0.97$ and RMSE= 8.47 l/h. The best ANN alternative (cascade CF) achieves close results with an $R^2 = 0.95$ and RMSE= 11.24 l/h.

However, the Poppe model reached such reliable prediction levels with a much lower number of tests, needing only 2. In comparison, the ANN alternatives need more data, at least 10 (with a good distribution over the operating range) for the FF and CF ANN models.

Air-cooled heat exchanger

Conclusions and recommendations

For the proposed optimization strategy in Section ?? (??), a fast, reliable model that can be scaled to different system sizes is required.

On the one hand, the first-principle models execution time is much higher than the data-driven alternatives, which is a significant drawback when it comes to the optimization strategy, where the model is evaluated many times in a short period of time. On the other hand, the data-driven counterparts are only applicable to the conditions and the particular system with which they are developed.

Conversely, one of the main strengths of both physical models presented in this chapter, is their ability to predict the operation of the coolers regardless of the conditions tested; while the data-driven execution time is faster by orders of magnitude, it can be vectorized and its execution time is more constant regardless of the input conditions.

Therefore, as combining a wet cooler and a dry cooler into a combined cooler offers potential advantages compared to the individual systems, combining both modelling approaches is the chosen solution to model the system. The best performing data-driven model, the Gaussian-Process Regression (GPR) is calibrated using data from the first-principle models, where physical models are adapted dynamically to the required scale and finally the data-driven model can be generated. This approach provides a way of having on-demand models that can be adapted to the particular case study, while still being fast and efficient in terms of computational resources.

14.1.4 Condenser model validation

For the surface condenser[4] a physical model is used, with the heat transfer coefficient as the only parameter to calibrate. Seven different alternative estimations of the heat transfer coefficient were calculated, using the data from the experimental campaign described in Section ?? (??). They are as follows:

4: See Section ?? (??)

1. Empirical correlation using the condenser flow rate (q_c) and the vapor temperature (T_v) as inputs.
2. Empirical correlation using the cooling water inlet temperature ($T_{c,in}$) and T_v as inputs.
3. Empirical correlation using the flow rate per condenser tube ($q_{c,tube} = q_c/n_{tubes} = q_c/24$) and the cooling water inlet temperature.
4. Nominal value from the manufacturer, which equals 1.838 W/m^2 °C
5. Calibra_Uexp_original
6. Calibra_Uexp_recortado

Estos qué son? Generar una nueva versión de la figura una vez se seleccionen los métodos finales

The results of the calibration are shown in Figure 14.8, where the y-axis shows the thermal power obtained and the x-axis holds different bars for the different heat transfer coefficient estimation methods, with bars also for the experimental heat released by the vapor and absorbed by the coolant. As can be seen in the figure. The shown results are for steady-state conditions with the condenser in an equilibrium state ($Q_{\text{released}} \approx Q_{\text{absorbed}}$), and with a large variation in the condenser conditions (120 to 200 kW, the whole operating range of the condenser). The results show that the heat transfer coefficient obtained with the method 3 is the one that best fits the experimental data, with a MAE of 17.6 kW and a maximum error of 33.41 kW (15%).

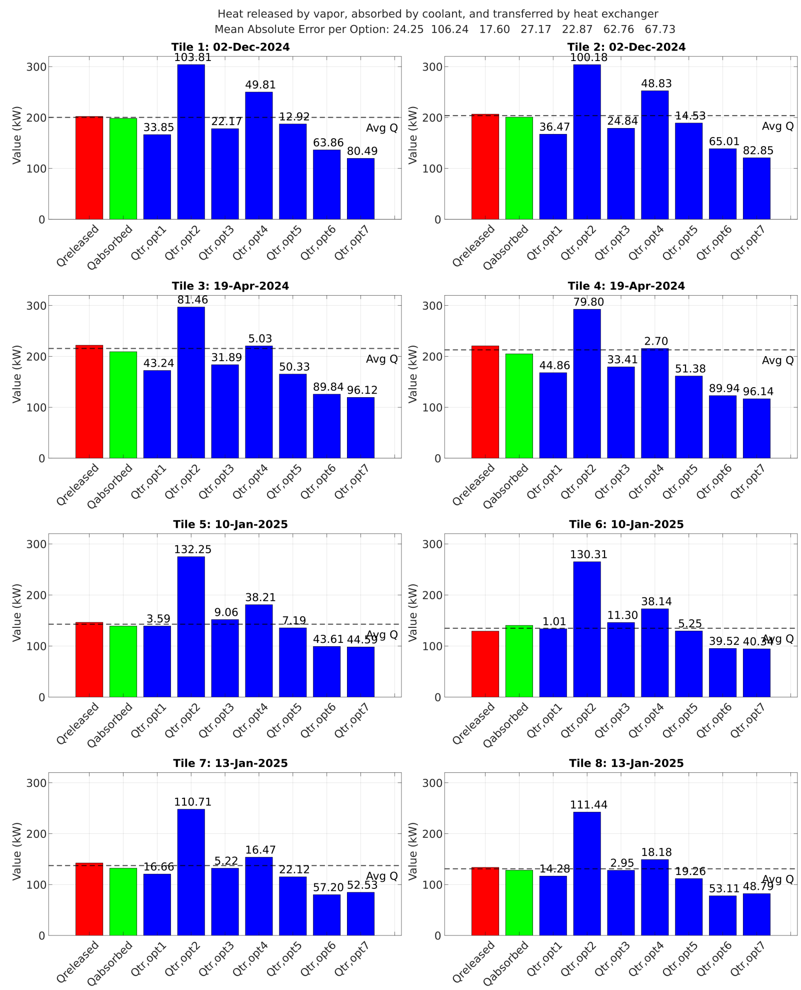

Figure 14.8: Heat transfer coefficient calibration results

14.1.5 Complete system model validation

Esto, o bien se hace comparando puntos en estático cuando todo el sistema está en estacionario, o en la gráfica de validación de la estrategia de optimización se muestra también una línea con las predicciones del modelo. Y después una tabla con cada una de las salidas del sistema, mostrando el error entre cada una de las predicciones del modelo (cada vez que se evalúa la optimización), en comparación al valor real obtenido en la planta.

a completar una vez se tengan resultados experimentales, hay que implementar la función para generar la visualización

Cuando haya un cambio en la planificación, las predicciones de predicciones antes a conocerse el cambio, cambiar su color a un gris para mostrar que esas predicciones ya no son válidas pues han cambiado las condiciones.

Figure 14.9 shows the model validation results for the complete system model. Different plots are shown for the main output variables[5]. Solid lines represent the measured variables in the real facility, while the different markers represent the predictions generated at different times. The plots also include a right-axis to display a metric error, specifically the MAPE of the predictions with respect to the measured values. The error is shown with a bar for each prediction.

5: C_w, $T_{dc,out}$, etc

The results show that the model is able to predict the main output variables of the system with a good accuracy. As expected the errors compound over time, specially after the change in the operation schedule at XX:XX. Nonetheless, the

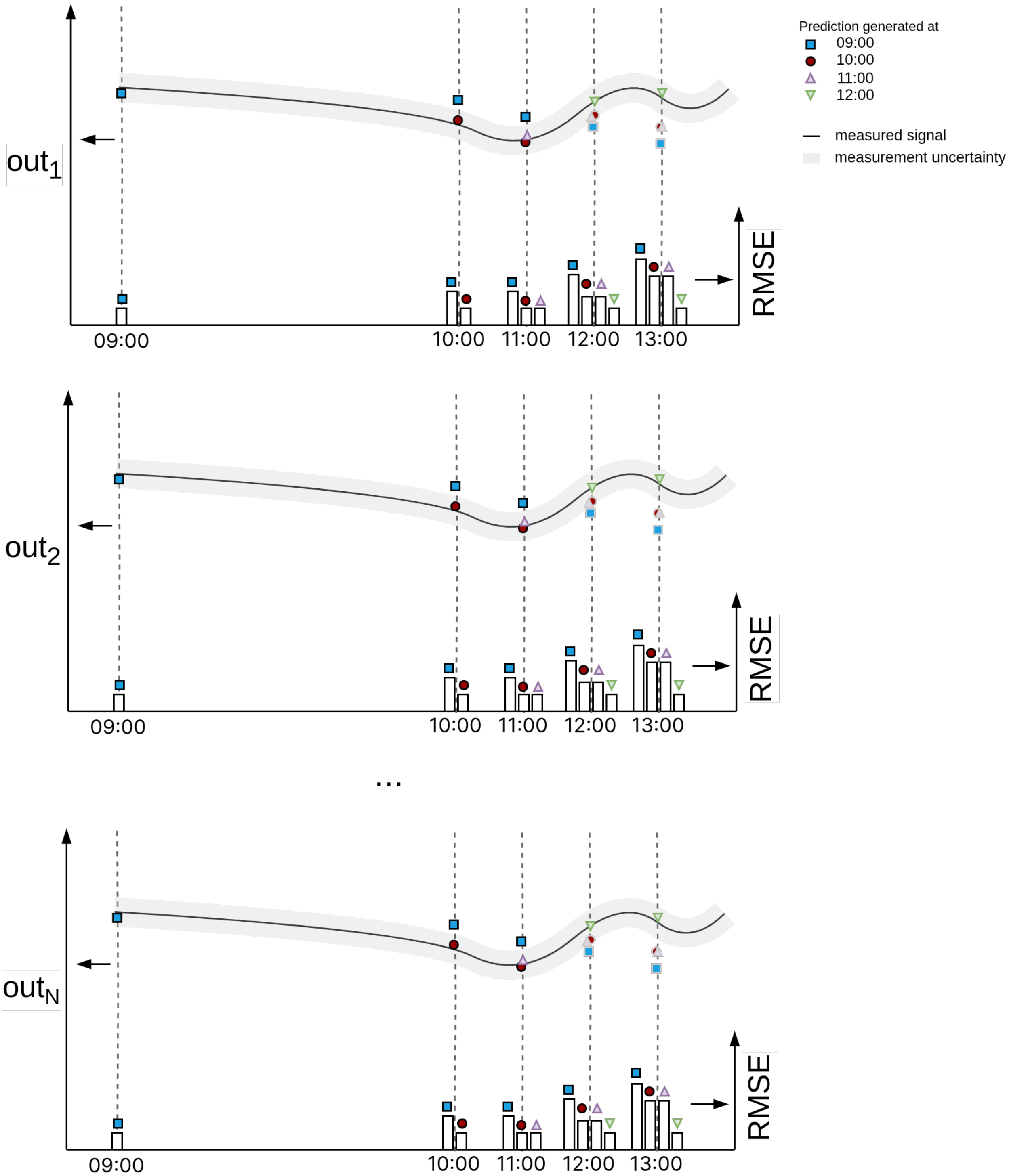

Figure 14.9: Figure caption.

model is able to adapt after a new evaluation including the change and overall predictions below XX% of error are achieved.

14.2 Control and optimization results

Once the models of the main components of the system have been validated, the next step is to validate the optimization strategy proposed in Section **??** (**??**). First, an optimization algorithm is chosen by comparing different alternatives in Section 14.2.1 (Choosing an optimization algorithm). Then, the two proposed variants for the combined cooler are compared in simulation for one operation day in the simulated pilot plant in order to see which one performs better in Section 14.2.2 (Comparing the static and horizon optimization strategies). Finally, two validation scenarios are tested in the real facility, one where a regular operation schedule is followed throughout the operation, and a second one where planned changes are introduced in the operation schedule, in order to validate how the optimization strategy adapts to changing conditions.

14.2.1 Choosing an optimization algorithm

Static problems

For every static optimization problem (referencias a problemas) four different algorithms were tested: (N+1)-ES Simple Evolutionary algorithm (SEA), Improved Harmony Search algorithm (IHS) and Differential Evolution with Constraint Handling algorithm (DE-CSTR). For each alternative the same number of objective function evaluations were given, XX. For each alternative three options are tested with a different population .... Table X shows the results obtained, in terms of fitness at different stages in the evolution. From the results it can be seen that for all alternatives the best performing and most consistent algorithm is ...

Horizon optimization. Path selection

A methodology similar to the static comparison is used. This time the algorithms evaluated are: Generalized Ant Colony Optimization algorithm (GACO), IHS, Simple Genetic Algorithm (SGA) and Particle Swarm Optimization algorithm (PSO). Three different population sizes are tested (80, 150 and 1000) if the particular algorithm evolves more than one individual; the number of generations is calculated accordingly so that all alternatives have the same budget of objective function evaluations, equal to 200k evaluations[6]. The results are visualized in Figure 14.10, where there are different plots for different dates, the y-axis represents the fitness and the x-axis shows the number of objective function evaluations. The results show that consistently the SGA outperforms the alternatives, and particularly, the smaller population size (80) configuration followed very closely by the 150 population size configuration.

6: Only up to 50k evaluations is shown in the figure for clarity

14.2.2 Comparing the static and horizon optimization strategies

TODO

Poner la figura de resultados del horizonte para SOLO un día detallado aquí (más días hace que no se distingan bien las barras, tampoco se puede poner el pareto). Debe incluir la distribución hidráulica en barras comparando estático con horizonte, el frente de pareto del horizonte, y la comparativa de coste acumulado.

La figura es provisional. Actualizar la figura con cambios mencionados

Comentar la figura, sobre el frente de pareto que se muestra, cómo la estática al principio abusa del agua y para el final del día aumenta muchos sus costes, etc.

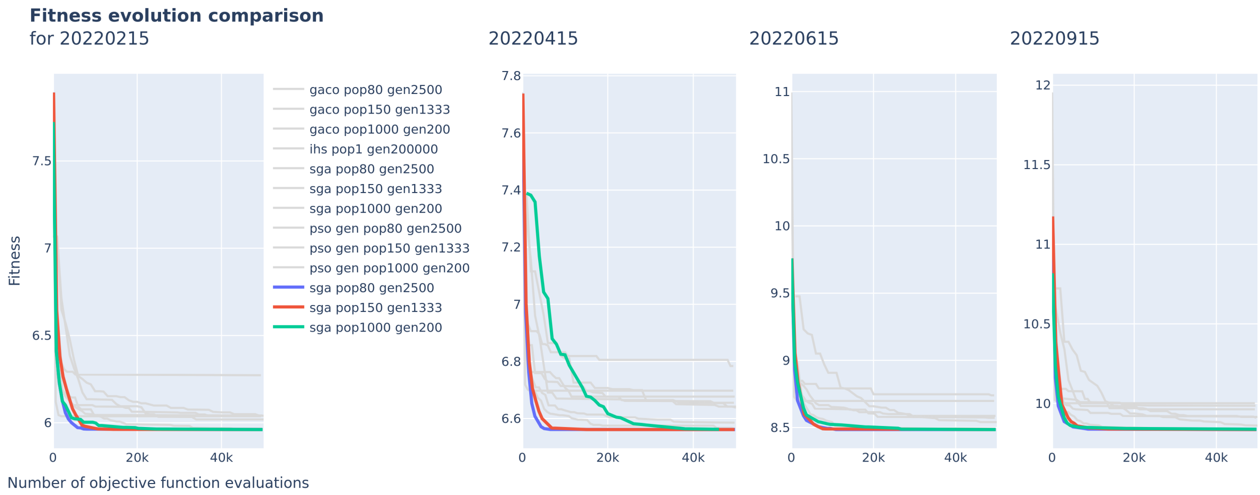

Figure 14.10: Horizon optimization – path selection subproblem. Fitness evolution comparison for different algorithms in four different dates.

14.2.3 Validation at pilot plant

A hierarchical control strategy has been implemented in order to validate the optimization strategy in the real facility. Figure 14.12 shows a diagram of the methodology, where the left side represents the upper layer with the proposed shrinking horizon optimization[7] and the right side shows the low-level regulatory control layer, which directly interfaces with the actuators and sensors of the facility.

7: See Section ?? (??)

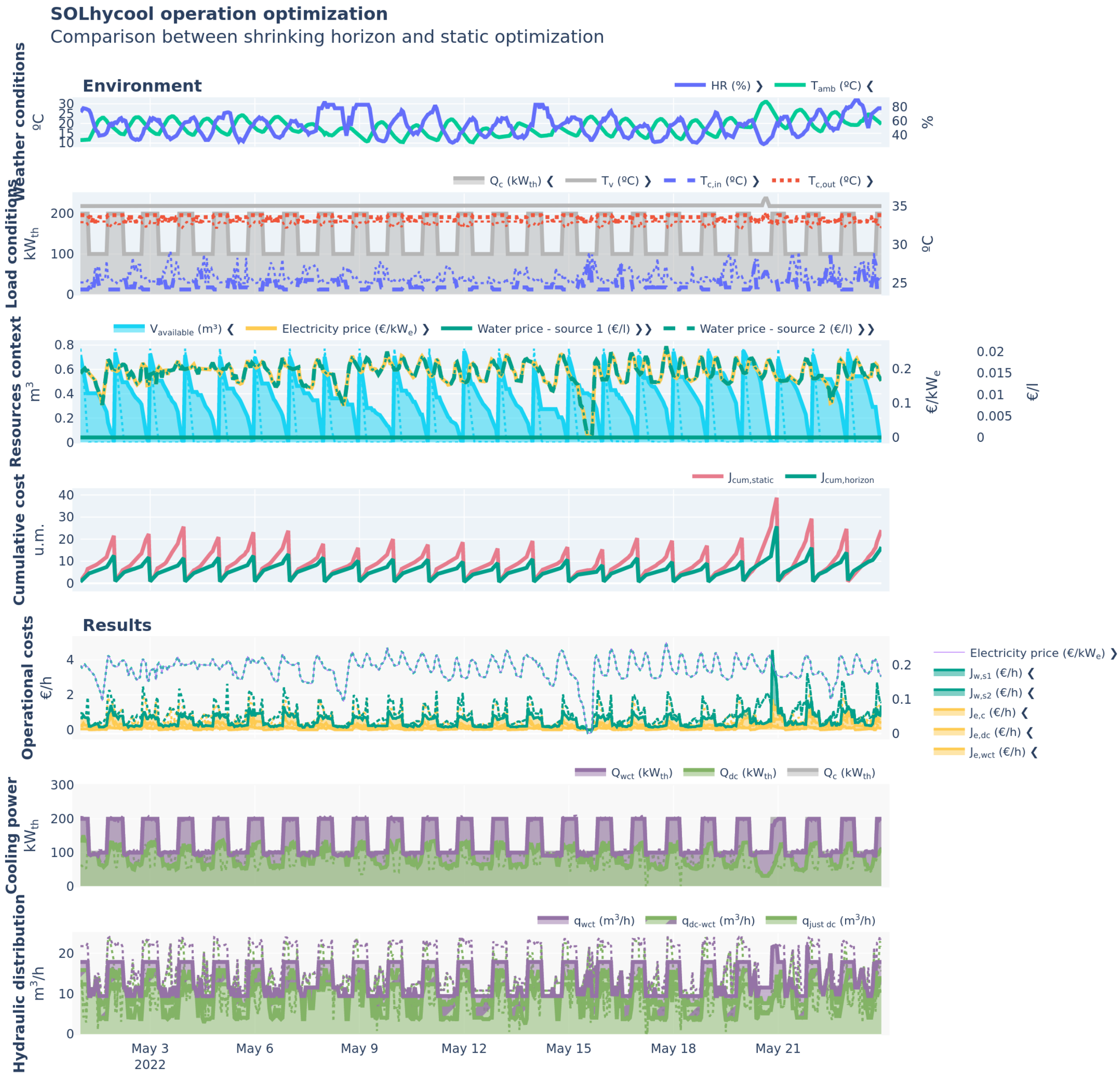

Figure 14.11: Detailed simulation results for the horizon optimization compared to the static alternative.

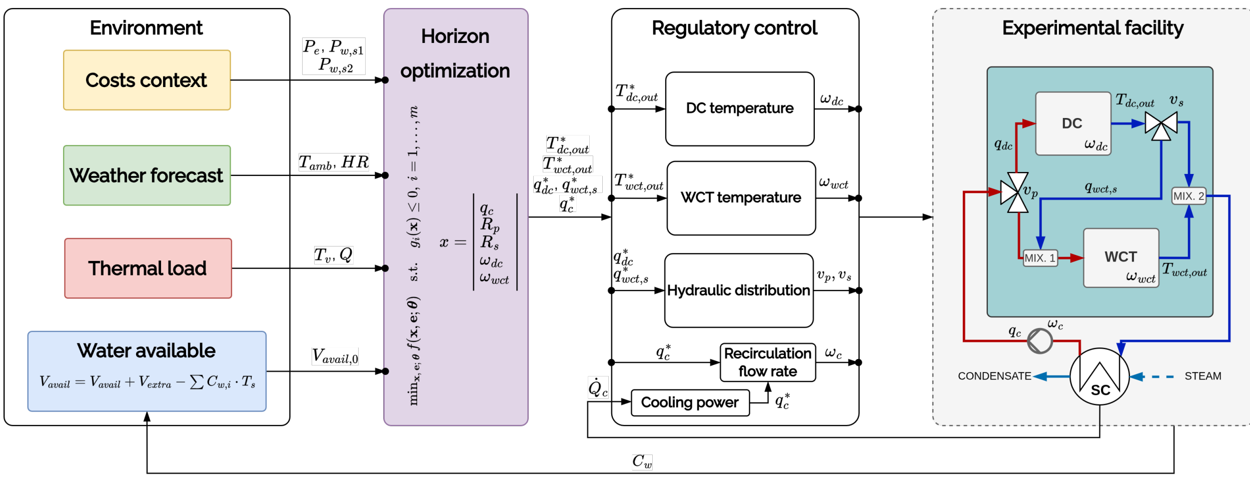

Figure 14.12: Implementation of the optimization strategy in the real facility. Hierarchical control

Table 14.5: Box-bounds for the decision variables.

$\mathbf{x}$	Units	lb	ub
q_c	m^3/h	5.22	24.15
R_p	–	0.00	1.00
R_s	–	0.00	1.00
ω_{dc}	%	11.00	99.18
ω_{wct}	%	21.00	93.42

openweater_api

Environment. To generate the environment for the optimization, weather forecasts using the OpenWeather API were used[**openweater_api**], for the electricity costs data from the 2022 spanish grid was used, updating the year to the one in which the experiment was performed, and the water cost was set to $C_{w,s1} = X$ and $C_{w,s2} = Y$. For the thermal load a profile was generated by setting a constant vapor temperature of $T_v = 45\,^{\circ}$C while an arbitrary cooling power was generated considering the heat availability from the flat-plate collector field, which is the heat source of the system, for the particular day. Finally, an initial value for the water availability was set to $V_{avail,0} = 0.5\,m^3$, and from there it is updated by reading the actual system consumption online.

Optimization layer. The optimization algorithm is run every 30 minutes, and generates a new set of results for the remaining operation time. The results of the optimization are then passed to the regulatory control layer by setting them as setpoints for the low-level control. The box-bounds for the decision variables are shown in Table 14.5.

aiuda Lidia!

Control layer. Four controllers are implemented in this layer...

Annual analysis: ANDASOL-II CSP plant 15

TL;DR

This chapter presents the annual simulation results for different cooling systems: a WCT, a DC and the presented CC optimized with static optimization and with horizon optimization. They provide cooling to the power block of the XX hours storage–CSP plant ANDASOL-II with an off-peak operation strategy. Results for the case study report a specific cooling cost of XX, XX and XX for the WCT, DC and CC, respectively, compared to the 5 L/kWh figure provided by the developer.

Introduction

A modeling framework has been developed to simulate and optimize the operation of various cooling systems, with a particular focus on the proposed combined cooling system. This methodology has been validated using data from a pilot plant. In this chapter, the objective is to apply the framework to a specific case study: a CSP plant.

As previously mentioned, CSP plants are among the most water-intensive power generation technologies [36], a concern that is especially relevant in the arid regions where they are typically located. To assess the performance-water use and operational costs- of different cooling systems, the proposed methodology is applied to a real-world case study through an annual simulation. The case study examined is the Andasol-II CSP plant.

Figure 15.1: Andasol I, II and III aerial view. Andasol II is the one at .
Source: https://en.wikipedia.org/wiki/File:Andasol_5.jpg

[36]: Meldrum et al. (2013), "Life cycle Water Use for Electricity Generation"

In the south-east of Spain, near Guadix and next to the Sierra Nevada mountain range (see Figure 15.1), thanks to the region high altitude (1100 m) and the semi-arid climate, the site has exceptionally high annual direct insolation (2260 W/m^2) and thus is ideal for solar projects. This is why the first parabolic trough power plant in Europe, Andasol-I, was built there in 2008. One year later Andasol-II followed, located in the immediate neighbourhood and with almost identical construction. It has a rated output of 50 MW with 7.5 hours[1] of thermal storage, providing electricity for up to 200,000 people. More specifications are available in Table 15.1.

1: This means that if fully charged, it can produce the nominal rated power of the turbine for that duration

According to the developer, Andasol-II vaporizes 870 000 m^3/year, or in specific units **5 l/kWh**.

Table 15.1: ANDASOL-II plant main characteristics

Technology	Parabolic Trough
Solar Resource	2260 W/m^2
Nominal Capacity	50 MW
Status	Operational
Start Year	2009
TF Inlet Temperature	293°C
TF Outlet Temperature	393°C
Power Cycle	Steam Rankine
Turbine Efficiency	38.1%
Cooling Type	Wet
Storage Type	Molten salts
Storage Capacity	7.5 Hours – 1 GWh

Source: Institute for Advanced Sustainability Studies (IASS) and others, 2022; data by Lilliestam@IASS, Thonig@IASS, Zang@CAS, Gilmanova@CAS and others.

15.1 Limitations

Considerar mover esto al apartado de trabajos futuros

1. The combined cooler analyzed has a 50% split in nominal cooling power of the WCT and DC components compared to the standalone cooling systems. Different ratios could be analyzed and one would probably be a better fit for the particular case study. This in itself is a design optimization problem that is not addressed in this thesis.
2. An ACHE is used for the DC, but other options could be considered, such as an ACC.

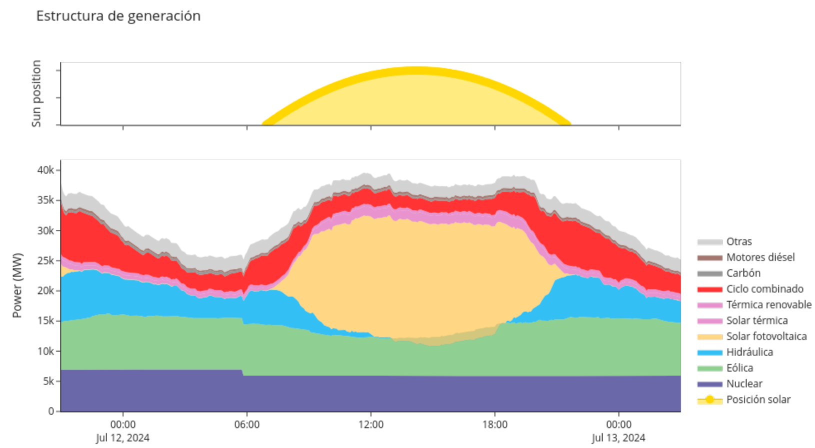

Figure 15.2: Spanish electricity mix on July 12, 2024. The peak in photovoltaic generation is clearly visible at midday, while thermosolar generation is more evenly distributed throughout the day. Peak production is majorly from CSP plants with no storage.
Data source: Figure elaborated using data extracted from `https://www.ree.es/es/datos`

15.2 Environment definition

15.2.1 Water context

Obtaining accurate water availability data is challenging. Unlike resources such as electricity—where demand, supply, and prices are readily available—water availability data is often lacking. Water prices are not standardized; they vary from region to region, and even within the same region, depending on the source and the specific agreements in place.

For the simulation scenario, two sources of water are considered[2]. The first source is rainwater or water from a dam, which is assumed to be available at a constant price of XX [**<empty citation>**]. To create a representative dataset, water availability is modeled as a function of precipitation data, which can be obtained from hourly Typical Meteorological Year (TPY) data [**meteonorm_**]. A linear model is fitted to relate maximum precipitation to maximum available water, and when there is no precipitation, water availability is set to zero. The data is then resampled every 15 days, and the daily volume of available water is calculated by dividing the resampled fortnightly volume by 15. This approach accounts for the presence of water reservoirs and some degree of management capacity.

2: See Section **??** (**??**)

<empty citation>

meteonorm_

The alternative source is regenerated water[3] is not limited in volume.

3: This is not an exogenous idea; the Villena CSP plant, for example, uses wastewater from a nearby prison to partially meet its water needs [**<empty citation>**]

15.2.2 Thermal load

Traditionally, thermal power plants were designed and operated to generate electricity only when solar energy was available. This approach remained common until the rapid rise in competitiveness of Photovoltaic (PV) plants, which offer significantly lower generation costs. In response, concentrated solar power plants began integrating thermal energy storage systems to enable dispatchable power generation. Today, 21 out of 51 CSP plants in Spain—approximately 42%—have thermal storage capacities exceeding two hours [2, 37, 38]. This enables them to produce electricity even when solar input is unavailable.

[2]: Thonig et al. (2023), *CSP.Guru 2023-07-01*

[37]: Lilliestam et al. (2021), "The Near- to Mid-Term Outlook for Concentrating Solar Power: Mostly Cloudy, Chance of Sun"

[38]: Bonilla et al. (2024), "CSP Data: A Data Discovery Web Application of Commercial CSP Plants"

However, many of these plants still follow traditional operating patterns, generating most of their electricity during peak solar hours[4]. This strategy is increasingly seen as suboptimal and is likely to be phased out as the electric grid becomes saturated with PV generation[5].

4: The storage is primarily used to extend generation past sunset.

5: This trend is already observable in Spain during the summer months; see Figure 15.2

In this work, a different operational strategy is adopted: the plant is configured to generate electricity during off-peak solar hours, typically in the evening when electricity demand is at its highest. This is achieved by shifting the plant's production to align with these peak demand periods.

A model of the Andasol-II plant, developed by Bartolomé et al. [**<empty citation>**], was configured to follow this production strategy and simulated over an entire year. The resulting thermal load profile represents the demand to be met by the cooling system. The simulation used the same weather dataset as that employed for modeling the cooling system.

<empty citation>

15.2.3 Costs context

Electricity. The spanish grid operator Red Eléctrica de España (REE) provides an API[6] to access the electricity market prices. A python script was developed to systematically download monthly data[7] for each month in the desired year. The data is fetched in hourly intervals and saved in JSON format, then every file is read and joined into a single dataset resulting in prices for the whole year.

Water. Rainwater has a constant lower price of XX. This price was obtained considering that the plan has access to the same water than the irrigation community of the area[**<empty citation>**]. The alternative source, *i.e.* regenerated water, is considerably more expensive, and its price is linked to the electricity price, specifically by a factor of XX[8].

6: https://api.esios.ree.es

7: Longer periods would result in silent errors in the API

<empty citation>

8: This value includes a scaling factor to normalize the values

Simulation data and parameters information

Weather data	Hourly weather data from TPY of Guadix (Spain) for the year. Data was obtained from ...
Thermal load	Hourly thermal load data from the power block of ANDASOL-II CSP plant from a simulation model.
Electricity price	Spanish electricity market from 2022.
aximum available water	The maximum available water for ...
ative water source factor	...

The full environment dataset is available at

15.3 Optimization strategies comparison

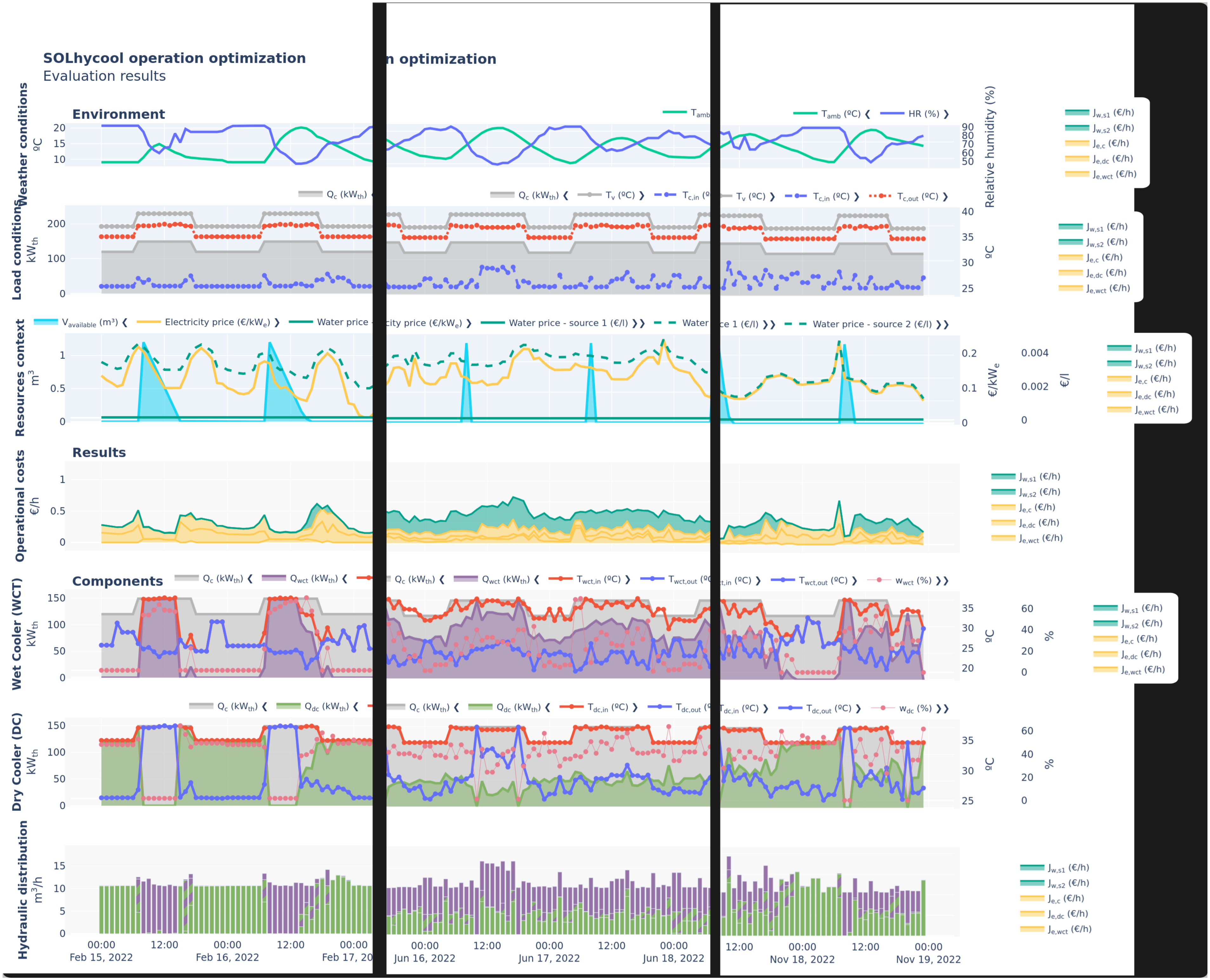

SOLhycool operation optimization
Evaluation results
Environment
Weather conditions
ºC
Relative humidity (%)
Load conditions
kWth
Resources context
m³
€/kWe
€/l
Results
Operational costs
€/h
Components
Wet Cooler (WCT)
Dry Cooler (DC)
Hydraulic distribution
m³/h
Feb 15, 2022
Feb 16, 2022
Jun 16, 2022
Jun 17, 2022
Jun 18, 2022
Nov 18, 2022
Nov 19, 2022

Figure 15.4: A rotated figure

15.4 Alternatives comparison

ca de barras compara-
or kWh refrigerado

ca de barras compara-
ución de potencia tér-
omponente y distribu-
lica por componente
ic y cc-horizon

Fusionar las gŕacias de resultados anuales remuestreados para que incluyan todas las alternativas. Cambiar fondo para cada sistema

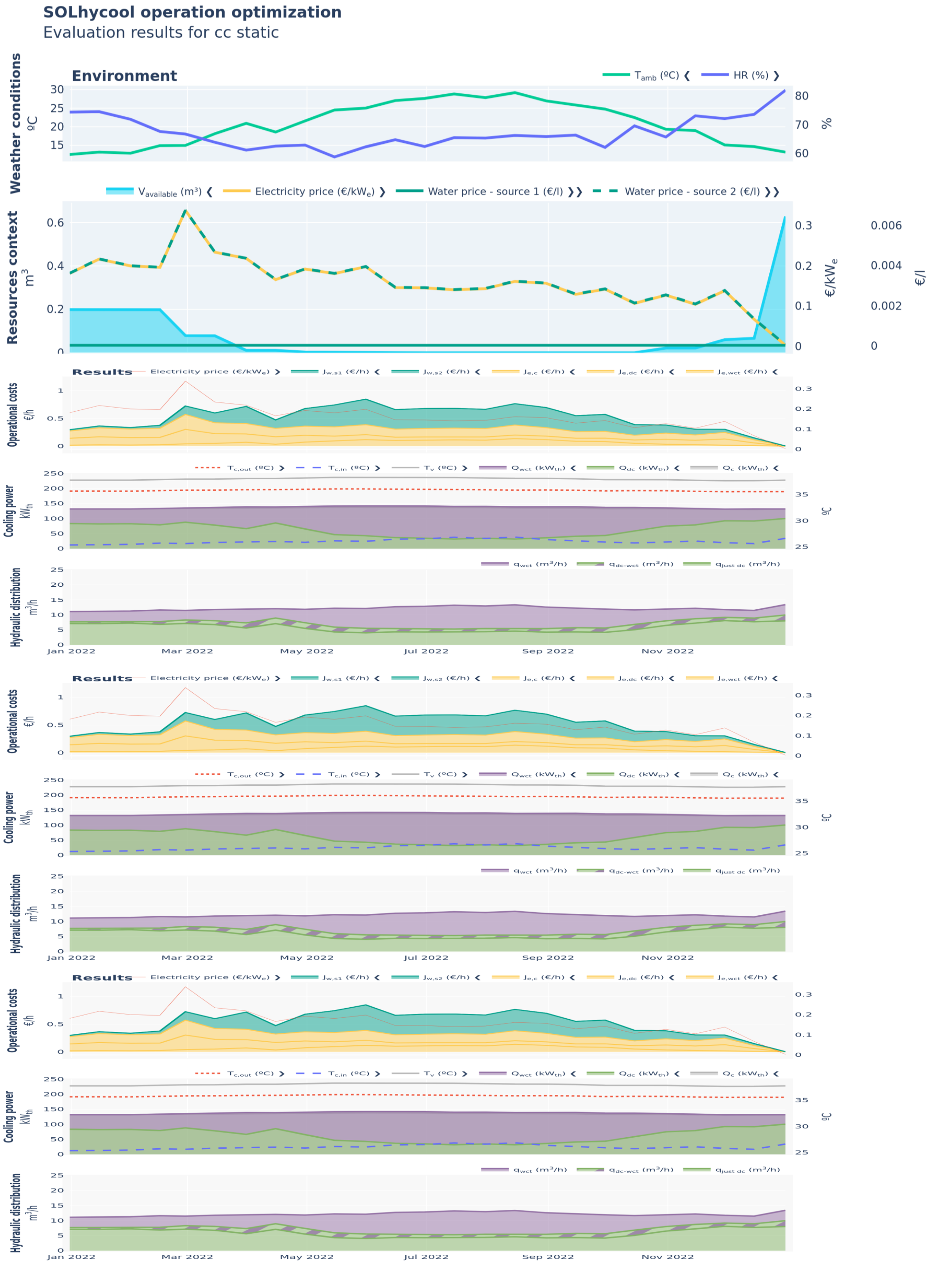

Figure 15.5: Annual simulation r
system optimized with static c
sults are resampled every 15
mean values. The original frequ
be found in the interactive vers

Conclusions and outlook

Conclusions

Outlook and future work

Optimal water and electricity management in a combined cooling system

Improved Pareto front computation. In the current optimization implementation, the Pareto front for each step in the optimization horizon is constructed using a grid search over the decision space. This approach can become computationally expensive, especially as the grid resolution increases. Additionally, the Pareto front must be recalculated from scratch at every step, even though the sequential steps are often very similar—cost parameters remain constant, and only the thermal load and weather conditions change, typically with small variations. A more efficient solution would be to use a multi-objective optimization algorithm such as NSGA-II [<empty citation>], which can transfer evolved populations between successive evaluations, significantly reducing redundant computations.

<empty citation>

Better water management In the current implementation, the primary water source is distributed evenly each day, so the optimization process uses up the entire supply daily. However, a more intelligent daily distribution—essentially, a new optimization problem—could improve water management by allocating different amounts on different days, based on expected weather conditions and predicted generation. This approach would likely be incorporated as a new layer in the hierarchical control structure.[9]

9: The resulting structure would be: 1. Water allocation, 2. CCS operation optimization, 3. CC regulatory control.

Techno-economic analysis. The presented cooling alternatives comparative in this thesis focus on the operation cost of the system, but to get a better picture of the alternatives performance, a techno-economic analysis that includes the capital cost of the system and the expected lifetime of the components should be performed *i.e.* considering all costs associated with the system the plant's lifetime. This is currently being worked on as part of [SOLHycool], where the methodology presented here in terms of operation costs will be integrated in a techno-economic analysis for different case studies.

Energy management in MED processes driven by variable energy sources

Alternative configurations for an MED brine concentrator. Configuraciones alternativas para procesos MED para aplicaciones de concentración de salmueras: geometría variable de efectos, fuentes externas en efectos distintos al primero, acoplamiento con MSF para efectos posteriores.

Alternative configurations for solar-driven MED. Configuraciones alternativas para el proceso solar MED (almacenamiento con distintos puntos de carga y descarga, MED con distintos puntos de fuente externa, etc. Incluir diagrama de draw.io con las distintas configuraciones)

Derived scientific contributions

1. Publicaciones en revista
2. Contribuciones a congreso
3. Coloquios doctorales
4. Colaboraciones en proyectos de investigación
5. Estancias de investigación

6. Repositorios de código
7. Repositorios de datos
8. Herramientas interactivas
9. Contribuciones a librerías de código abierto?

Bibliography

Here are the references in citation order.

[1] IEA. *Energy Technology Perspectives*. IEA. 2014. URL: https://www.iea.org/reports/energy-technology-perspectives-2014 (visited on 11/30/2023) (cited on page 11).

[2] Richard Thonig, Alina Gilmanova, and Johan Lilliestam. *CSP.Guru 2023-07-01*. Zenodo, July 1, 2023. (Visited on 05/31/2025) (cited on pages 11, 74).

[3] Ebrahim Rezaei, Sirous Shafiei, and Aydin Abdollahnezhad. "Reducing Water Consumption of an Industrial Plant Cooling Unit Using Hybrid Cooling Tower." In: *Energy Conversion and Management* 51.2 (Feb. 1, 2010), pp. 311–319. DOI: 10.1016/j.enconman.2009.09.027. (Visited on 03/10/2023) (cited on page 13).

[4] Wanchai Asvapoositkul and Mantheerapol Kuansathan. "Comparative Evaluation of Hybrid (Dry/Wet) Cooling Tower Performance." In: *Applied Thermal Engineering* 71.1 (Oct. 5, 2014), pp. 83–93. DOI: 10.1016/j.applthermaleng.2014.06.023. (Visited on 03/10/2023) (cited on page 13).

[5] Hemin Hu et al. "Thermodynamic Characteristics of Thermal Power Plant with Hybrid (Dry/Wet) Cooling System." In: *Energy* 147 (Mar. 15, 2018), pp. 729–741. DOI: 10.1016/j.energy.2018.01.074. (Visited on 03/10/2023) (cited on page 13).

[6] S. El Marazgioui and A. El Fadar. "Impact of Cooling Tower Technology on Performance and Cost-Effectiveness of CSP Plants." In: *Energy Conversion and Management* 258 (Apr. 15, 2022), p. 115448. DOI: 10.1016/j.enconman.2022.115448. (Visited on 03/29/2024) (cited on page 13).

[7] G. Barigozzi, A. Perdichizzi, and S. Ravelli. "Wet and Dry Cooling Systems Optimization Applied to a Modern Waste-to-Energy Cogeneration Heat and Power Plant." In: *Applied Energy* 88.4 (Apr. 1, 2011), pp. 1366–1376. DOI: 10.1016/j.apenergy.2010.09.023. (Visited on 03/10/2023) (cited on page 13).

[8] G. Barigozzi, A. Perdichizzi, and S. Ravelli. "Performance Prediction and Optimization of a Waste-to-Energy Cogeneration Plant with Combined Wet and Dry Cooling System." In: *Applied Energy* 115 (Feb. 15, 2014), pp. 65–74. DOI: 10.1016/j.apenergy.2013.11.024. (Visited on 03/10/2023) (cited on page 13).

[9] Patricia Palenzuela et al. "Experimental Assessment of a Pilot Scale Hybrid Cooling System for Water Consumption Reduction in CSP Plants." In: *Energy* 242 (Mar. 1, 2022), p. 122948. DOI: 10.1016/j.energy.2021.122948. (Visited on 03/10/2023) (cited on page 13).

[10] Faisal Asfand et al. "Thermodynamic Performance and Water Consumption of Hybrid Cooling System Configurations for Concentrated Solar Power Plants." In: *Sustainability* 12.11 (2020). DOI: 10.3390/su12114739 (cited on page 13).

[11] Raniyah Wazirali et al. "State-of-the-Art Review on Energy and Load Forecasting in Microgrids Using Artificial Neural Networks, Machine Learning, and Deep Learning Techniques." In: *Electric Power Systems Research* 225 (Dec. 1, 2023), p. 109792. DOI: 10.1016/j.epsr.2023.109792. (Visited on 03/31/2024) (cited on page 13).

[12] Martin T. Hagan et al. *Neural Network Design*. Martin Hagan, 2014. 800 pp. (cited on pages 16, 17).

[13] Mark Hudson Beale, Martin T Hagan, and Howard B Demuth. "Neural Network Toolbox." In: *User's Guide, MathWorks* 2 (2010), pp. 77–81 (cited on page 17).

[14] Lonnie Hamm, B. Wade Brorsen, and Martin T. Hagan. "Comparison of Stochastic Global Optimization Methods to Estimate Neural Network Weights." In: *Neural Processing Letters* 26.3 (Dec. 1, 2007), pp. 145–158. DOI: 10.1007/s11063-007-9048-7. (Visited on 03/16/2024) (cited on page 17).

[15] Jiri Nossent, Pieter Elsen, and Willy Bauwens. "Sobol'sensitivity Analysis of a Complex Environmental Model." In: *Environmental Modelling & Software* 26.12 (2011), pp. 1515–1525 (cited on page 19).

[16] Jon Herman and Will Usher. "SALib: An Open-Source Python Library for Sensitivity Analysis." In: *The Journal of Open Source Software* 2.9 (Jan. 2017). DOI: 10.21105/joss.00097 (cited on page 19).

[17] Takuya Iwanaga, William Usher, and Jonathan Herman. "Toward SALib 2.0: Advancing the Accessibility and Interpretability of Global Sensitivity Analyses." In: *Socio-Environmental Systems Modelling* 4 (May 2022), p. 18155. DOI: 10.18174/sesmo.18155 (cited on page 19).

[18] F. Merkel. "Verdunstungskühlung." In: *VDI Zeitschriff Deutscher Ingenieure, Berlin, Alemania* (1925), pp. 123–128 (cited on pages 33, 35).

[19] C Bourillot. “Hypotheses of Calculation of the Water Flow Rate Evaporated in a Wet Cooling Tower.” In: (Aug. 1983) (cited on page 33).

[20] H. Jaber and R. L. Webb. “Design of Cooling Towers by the Effectiveness-NTU Method.” In: *Journal of Heat Transfer* 111.4 (Nov. 1989), pp. 837–843. DOI: 10.1115/1.3250794 (cited on page 33).

[21] M. Poppe and H. Rögener. “Berechnung von Rückkühlwerken.” In: *VDI wärmeatlas* (1991), p. Mi 1 (cited on pages 34, 35).

[22] J.C. Kloppers and D.G. Kröger. “A Critical Investigation into the Heat and Mass Transfer Analysis of Counterflow Wet-Cooling Towers.” In: *International Journal of Heat and Mass Transfer* 48.3 (2005), pp. 765–777 (cited on page 34).

[23] C. G. Cutillas et al. “Energetic, Exergetic and Environmental (3E) Analyses of Different Cooling Technologies (Wet, Dry and Hybrid) in a CSP Thermal Power Plant.” In: *Case Studies in Thermal Engineering* 28 (Dec. 1, 2021), p. 101545. DOI: 10.1016/j.csite.2021.101545. (Visited on 03/27/2024) (cited on page 34).

[24] M. Hosoz, H. M. Ertunc, and H. Bulgurcu. “Performance Prediction of a Cooling Tower Using Artificial Neural Network.” In: *Energy Conversion and Management* 48.4 (Apr. 1, 2007), pp. 1349–1359. DOI: 10.1016/j.enconman.2006.06.024. (Visited on 03/08/2023) (cited on pages 34, 54).

[25] Ming Gao et al. “Artificial Neural Network Model Research on Effects of Cross-Wind to Performance Parameters of Wet Cooling Tower Based on Level Froude Number.” In: *Applied Thermal Engineering* 51.1 (Mar. 1, 2013), pp. 1226–1234. DOI: 10.1016/j.applthermaleng.2012.06.053. (Visited on 03/08/2023) (cited on page 34).

[26] Jialiang Song et al. “A Novel Approach for Energy Efficiency Prediction of Various Natural Draft Wet Cooling Towers Using ANN.” In: *Journal of Thermal Science* 30.3 (May 2021), pp. 859–868. DOI: 10.1007/s11630-020-1296-0. (Visited on 03/04/2023) (cited on page 34).

[27] P. Navarro et al. “Critical Evaluation of the Thermal Performance Analysis of a New Cooling Tower Prototype.” In: *Applied Thermal Engineering* 213 (2022), p. 118719. DOI: 10.1016/j.applthermaleng.2022.118719 (cited on pages 34–36).

[28] Ashrae. “HVAC Systems and Equipment.” In: *Chapter 36 Cooling Towers*. 2004 (cited on pages 36, 53).

[29] Lidia Martín and Mariano Martín. “Optimal Year-Round Operation of a Concentrated Solar Energy Plant in the South of Europe.” In: *Applied Thermal Engineering* 59.1 (Sept. 25, 2013), pp. 627–633. DOI: 10.1016/j.applthermaleng.2013.06.031. (Visited on 06/13/2025) (cited on page 41).

[30] Mariano Martín. “Optimal Annual Operation of the Dry Cooling System of a Concentrated Solar Energy Plant in the South of Spain.” In: *Energy* 84 (May 1, 2015), pp. 774–782. DOI: 10.1016/j.energy.2015.03.041. (Visited on 06/12/2025) (cited on page 41).

[31] David Wales and Jonathan Doye. “Global Optimization by Basin-Hopping and the Lowest Energy Structures of Lennard-Jones Clusters Containing up to 110 Atoms.” In: *The Journal of Physical Chemistry A* 101.28 (July 1, 1997), pp. 5111–5116. DOI: 10.1021/jp970984n. (Visited on 06/11/2025) (cited on page 47).

[32] UNE. *Thermal Performance Acceptance Testing of Mechanical Draught Series Wet Cooling Towers*. manual. UNE. 2004 (cited on page 53).

[33] CTI. *Code Tower, Standard Specifications. Acceptance Test Code for Water Cooling Towers*. manual. Cooling Technology Institute. 2000 (cited on page 53).

[34] Juan Miguel Serrano et al. “Wet Cooling Tower Performance Prediction in CSP Plants: A Comparison between Artificial Neural Networks and Poppe’s Model.” In: *Energy* (May 29, 2024), p. 131844. DOI: 10.1016/j.energy.2024.131844. (Visited on 05/30/2024) (cited on page 53).

[35] J. Ruiz et al. “Thermal Performance and Emissions Analysis of a New Cooling Tower Prototype.” In: *Applied Thermal Engineering* (2022), p. 118065. DOI: 10.1016/j.applthermaleng.2022.118065 (cited on page 60).

[36] J Meldrum et al. “Life Cycle Water Use for Electricity Generation: A Review and Harmonization of Literature Estimates.” In: *Environmental Research Letters* 8.1 (Mar. 2013), p. 015031. DOI: 10.1088/1748-9326/8/1/015031. (Visited on 05/28/2025) (cited on page 73).

[37] Johan Lilliestam et al. “The Near- to Mid-Term Outlook for Concentrating Solar Power: Mostly Cloudy, Chance of Sun.” In: *Energy Sources, Part B: Economics, Planning, and Policy* 16.1 (2021), pp. 23–41. DOI: 10.1080/15567249.2020.1773580 (cited on page 74).

[38] Javier Bonilla et al. “CSP Data: A Data Discovery Web Application of Commercial CSP Plants.” In: (July 2024) (cited on page 74).

Alphabetical Index